HYDROGEN PRODUCTION BY PHOTOASSISTED WATER ELECTROLYSIS USING SEMICONDUCTORS FILMS OF Bi_2MNbO_7 (M= Al, Fe, Ga, In)

Kevin Leandro Rosas Barrera

UNIVERSIDAD INDUSTRIAL DE SANTANDER

FACULTAD DE INGENIERÍAS FISICOQUÍMICAS

ESCUELA DE INGENIERÍA QUÍMICA

BUCARAMANGA

2011

HYDROGEN PRODUCTION BY PHOTOASSISTED WATER ELECTROLYSIS USING SEMICONDUCTORS FILMS OF Bi_2MNbO_7 (M= Al, Fe, Ga, In)

Kevin Leandro Rosas Barrera, Ing.

Tesis presentada para obtener el título de:

Magíster en Ingeniería Química

Directores:

Julio Andrés Pedraza Avella, Dr.

Dionisio Laverde Cataño, Dr

UNIVERSIDAD INDUSTRIAL DE SANTANDER

FACULTAD DE INGENIERÍAS FISICOQUÍMICAS

ESCUELA DE INGENIERÍA QUÍMICA

BUCARAMANGA

2011

Dedicatoria

Este trabajo está dedicado a toda mi familia
A mi padre, Julio Rosas, a mis hermanos Nury y Yeison por ayudarme y brindarme siempre su apoyo incondicional

A mi sobrino Juanchis por sacarme siempre una sonrisa

Pero en especial, a las dos personas que más amo en este mundo:
A mi madre, Carmen Julia Barrera, por darme la vida, por amarme tanto y por ser la persona más generosa y maravillosa que he conocido
Y a mi hermoso hijo, Samuel Esteban, quien es la luz de mi vida y la bendición más grande que he recibido

Kevin Leandro Rosas Barrera

Agradecimientos

Son muchas las personas a las que debo agradecer por ayudarme y aportarme en la realización y culminación de este trabajo. Y como dicen por ahí “el orden de los factores no altera el producto” así que:

Gracias a Colciencias por el financiamiento del proyecto 1102-332-18533.y a la Universidad Industrial de Santander por el apoyo económico.

A los integrantes del grupo de investigación, GIMBA, quienes me acogieron, me aconsejaron y me guiaron con sus conocimientos y experiencias para la realización este trabajo: Prof. Dionisio Laverde, Prof. Julio Elias Pedraza, Prof. Martha Niño y Prof. Elcy Cordoba (quien amablemente me aconsejó y me regaló un espacio en su laboratorio). A mis amigos y compañeros: Prospero Acevedo, Jose Luis Ropero, Olger Mendoza, Nancy Diaz, Paola Ballén, Jennyfer Cortés, Mónica cardeño y Carolina Jaimes por su amistad, colaboración y participación de este trabajo.

A Julio Andrés Pedraza por su apoyo, por las noches de trabajo, por las ideas y aportes realizados. Julio, muchas gracias aprendí mucho de usted.

A Adriana Judith Becerra, por estar siempre pendiente de mi trabajo, alentándome y aconsejándome. Adriana gracias por su amistad y por todo lo que me enseñó.

A Eduardo y Wilson Carreño, por su infinito apoyo y colaboración. A Diana Consuelo Camargo por ayudarme en todo, soportarme y brindarme su amistad.

A mis grandes amigos, Oscar Emilio, Laura Liliana, Luisa Fernanda, Oscar Javier, Ximena Ramirez Pili Pineda, Deisy Corina, por su amistad, apoyo, comprensión, por los regaños y tiradas de orejas, pero sobre todo por regalarme un espacio en su vida. Los quiero mucho.

Al doctor Mario Álvarez, por hacerme sentir como de su familia, por enseñarme tantas cosas. Doctor Mario muchas gracias por creer en mí, por su apoyo y su amistad, por abrirme camino en el difícil mundo de la docencia y por ser un ejemplo a seguir. Soy muy afortunado de conocerlo y de poder compartir con usted muy buenos momentos y grandes experiencias.

A Diana Sofía, por darme el más grande y hermoso regalo.

Gracias a todas las personas que no alcancé a nombrar, que comparten conmigo el día a día y que han hecho parte de este trabajo, a todos ellos…infinitas gracias.

TABLE OF CONTENS

Chapter 5

LIST OF TABLES

LIST OF FIGURES

RESUMEN

TÍTUTULO: PRODUCCIÓN DE HIDRÓGENO POR ELECTROLYSIS FOTO-ASISTIDA DEL AGUA USANDO PELÍCULAS SEMICONDUCTORAS DE Bi_2MNbO_7 (M= Al, Fe, Ga, In)*

Autor: Kevin Leandro Rosas Barrera**

Palabras Claves: Óxidos complejos, Sistema Bi–M–Nb–O, Estructura tipo pirocloro, Películas semiconductoras, fotoánodos, Rompimiento fotoelectroquímico de agua.

En este trabajo de investigación, se estudió la producción de hidrógeno y la oxidación simultánea de de cianuro usando como fotoánodos películas de Bi_2MNbO_7 (M= Al, Fe, Ga, In,) sobre láminas de acero inoxidable AISI/SAE 304. Las películas fueron preparadas por sol-gel dip-coating y calcinadas a 500℃. Una celda electroquímica de dos compartimientos con cátodos de diferentes materiales (Plata, Platino y Acero inoxidable platinizado) fue empleada en la evaluación bajo diferente composición de electrolito. La corriente que circulaba, la generación de hidrógeno y la degradación de cianuro fueron monitoreadas en función del tiempo.

Los resultados muestran que la actividad de los fotoánodos de Bi_2MNbO_7/SS 304 fue más alta o equivalente al fotoánodo de TiO_2/SS 304 in el rompimiento fotoelectroquímico del agua. Además, se encontró que la actividad más alta en el proceso es fuertemente influenciada, sino determinada, por las propiedades locales de la interface semiconductor-electrolito y no por las características de transporte fotoeléctrico. Por otra parte, el empleo de un cátodo de platino en una solución alcalina (sin KCl) muestra valores más altos de velocidad de producción de hidrógeno y oxidación de cianuro con respecto a los resultados obtenidos con el cátodo de plata.

Finalmente, en todos los casos el valor más alto de la densidad de corriente y de la cantidad de hidrógeno producida fue obtenida usando acero inoxidable platinizado como cátodo. Siendo el fotoánodo de Bi_2InNbO_7 el que mostró la mayor actividad fotocatalítica.

---

*Trabajo de Investigación de Maestría en Ingeniería: Área Ingeniería Química.
**Facultad de Ingenierías Fisicoquímicas, Escuela de Ingeniería Química. Director: Julio Andrés Pedraza Avella, Ph.D. Director: Dionisio Antonio Laverde Cataño, Ph.D

ABSTRACT

TITLE: HYDROGEN PRODUCTION BY PHOTOASSISTED WATER ELECTROLYSIS USING SEMICONDUCTORS FILMS OF Bi_2MNbO_7 (M= Al, Fe, Ga, In)

Author: Kevin Leandro Rosas Barrera**

Keywords: Complex oxides, Bi–M–Nb–O system, Pyrochlore-type structure, Semiconductor films, Photoanode, Photoelectrochemical water splitting.

The hydrogen production and the simultaneous cyanide oxidation by a photoelectrocatalytic process was studied using Bi_2MNbO_7 (M = Al, Fe, Ga, In) films on AISI/SAE 304 stainless steel plates (SS) as photoanode. The films were prepared by sol-gel dip-coating and annealed at 500℃. A two-compartment electrochemical cell with cathodes of different materials (silver, platinum and platinized stainless steel) was employed in the evaluation under different electrolyte compositions. The circulating current, the hydrogen generation and the cyanide degradation were monitored at different times.

Results showed that the activity of Bi_2MNbO_7/SS 304 photoanodes in the photoelectrochemical water splitting was higher or equivalent than that of TiO_2/SS 304 photoanode. Furthermore, it was found that the higher activity in the photoelectrocatalytic process is strongly influenced, if not determined, by the local properties of semiconductor-electrolyte interface and not by the photoelectrical transport characteristic. The other hand, the use of a platinum cathode in an alkaline solution (without KCl) shows higher values of hydrogen production rate and cyanide oxidation with regard to obtained results with Ag cathode.

Finally, in all cases the highest value of current density and amount of hydrogen produced was obtained using the platinized stainless steel as cathode. Being the Bi_2InNbO_7 photoanode the most active.

---

* Thesis to obtain the degree of Master in Engineering, Area: Chemical Engineering.

** Faculty of Physical-chemical Engineering, Chemical Engineering School. Advisor: Julio Andrés Pedraza Avella, Ph.D. Advisor: Dionisio Antonio Laverde Cataño, Ph.D

INTRODUCTION

Around the world, many experts motivated by the need of develop cleaner energy alternatives and reduce the emission of greenhouse gases [1], perceive the possibility of use the energy derived of sun to mitigate some dependence of fossil fuels.

An alternative fuel based in solar energy, obtained of renewable and economic sources, is the hydrogen [2-5]. It is the most abundant gas in the world, the source of all energy that we receive from sun, highlighted by have the energetic content higher per unit weight and by generate water vapor as combustion product.

Although hydrogen is one of the elements most abundant over earth crust, it is not a primary energy source, that is, is not find as H_2, but it can be found combined with others elements as oxygen (to form water), and carbon and nitrogen in lightweight materials and fossil fuels; needing some physical chemical processes that involve the use of primary energy sources to be obtained. It is for this reason that hydrogen is not considered as an energy source, but as secondary energy carrier [6].

There are some ways to obtain hydrogen, since catalytic reforming with water vapor (process industrially more used) through a variety of technologies as process chemicals, biological, thermals, electrolytic, among other things. However, only some of them are environmentally friendly.

Alkaline water electrolysis, that it has been used for more than 80 years, is enough attractive because hydrogen and oxygen gases obtained are extremely pure. This technique involves the induction of an electric current through an electrolytic conductor, where an anode and cathode are immersed, to origin a transport of material (electrons) and produce a redox reaction. However, the cost of the hydrogen production is high because the process needs the application of an external potential to water split into its constituent elements [7].

There are some modifications of the traditional process that looking the consume decrease of electric energy during the electrolysis using a semiconductor material as photoanode. The process that is known as photoelectrolysis (photoassisted electrolysis of water), use the semiconductor material to absorb the energy derived of the sun to promote redox in the surface and generate an electric current that is transmitted to cathodic material to hydrogen generation. The absorption of light energy by the photoanode decreases the amount of electric

energy that it should apply to water splitting molecule, it making a more rentable process and one of the most promising alternatives in hydrogen production. [8]

This process began around 1970 with Fujishima and Honda [9], who use a TiO_2 photoelectrode and a platinum electrode as cathode in a cell called photoelectrochemical cell (PEC). Is worth nothing mentioned that while Fujishima and Honda did experimental test, Bockris[10] and Gerischer[11] establish scientists foundations of the photoelectrochemical hydrogen production; since then this reaction has been object of many investigators in different knowledge areas as photocatalysis, electrochemical, and materials science [12-14].

The water photoelectrolysis can take place with the help of the light on a material semiconductor, provided the conduction band potential of the semiconductor is more negative than the reduction potential of the water to form H2 (0 V vs. ENH to pH = 0) and the valency band potential of the semiconductor is more positive than the potential of oxidation of the water to form O2 (1.23 V vs. ENH to pH = 0).

For this reason, not all material can be used to hydrogen generation. Historically TiO_2 is the material that has attracted most interest in water photoelectrolysis [9, 15, 16]. However, from standpoint of hydrogen production it is not attractive, because the potential band conduction is not enough negative to the hydrogen evolution will be possible (H_2/H_2O) and also it need photons of high energy, with wavelengths in UV region, to the pairs of electron-hole can be generate [17-21] Additionally, the potential capacity that this material has to produce hydrogen from the water, disappear when the pairs of electron-hole are generated, since the activation of the semiconductor generate a shift in the levels of valence and conduction bands [22].

Some materials, as MoS_2, Fe_2O_3, In_2O_3, WO_3 y CdO, as well as TiO_2, do not have an enough negative conduction band to produce the hydrogen evolution, as is shown in figure 1. [23]

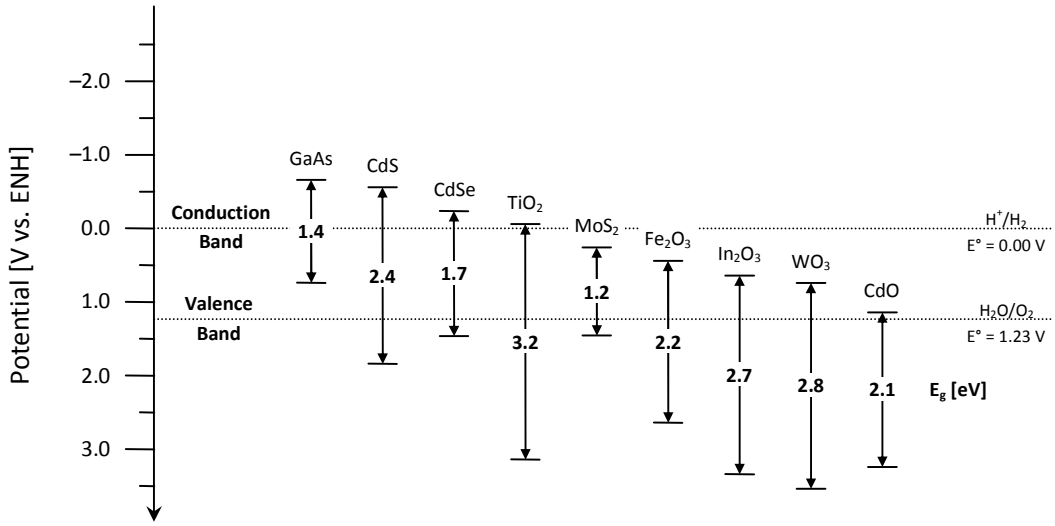

Figure 1 Potentials of valence and conduction bands and gaps between bands (E_g) different to typical semiconductors (pH = 0).

Other materials as GaAs y CdSe, with small band gaps make inefficient the water decomposition for its high recombination. On the contrary, those with wide band gaps between needs high energy photons not supplied by visible radiation to generate the respective pair electron-hole or simply photocorrosion factors or toxicity, delimited the application of photocatalysts as ZnO and CdS.

All these needs and limitations exposed previously, shown that is clue develop new materials to make feasible and economically viable the water photodecomposition. Also, the search should be directed to that these semiconductors absorb major quantity of solar energy and they shown an appropriate catalytic activity that favors the possible reaction that they will happen on its surface [24]. In this sense, a semiconductors materials series including trinitates, niobates and tantalates, with laminar or tuneladas structure perovskita type (ABO3: SrTiO3, NaTaO3, LaTiO3) and pyrochlore type ($A_2B_2O_7$: Bi_2MNbO_7 (M = Al, Ga, In, Y, Fe, Sm))[25], has been tested in hydrogen production, showing a high activity and propose them as appropriate materials to be applied in photoelectrochemical cells; because so far most of them have only been tested as photocatalysts in suspension [26].

In Figure 2 can be see the valence and conduction bands potentials determined theoretical form [27], of Bi_2MNbO_7 materials with pyrochlore structure types as well as the band gap. The materials pyrochlore type shows an appropriate position to hydrogen and oxygen evolution.

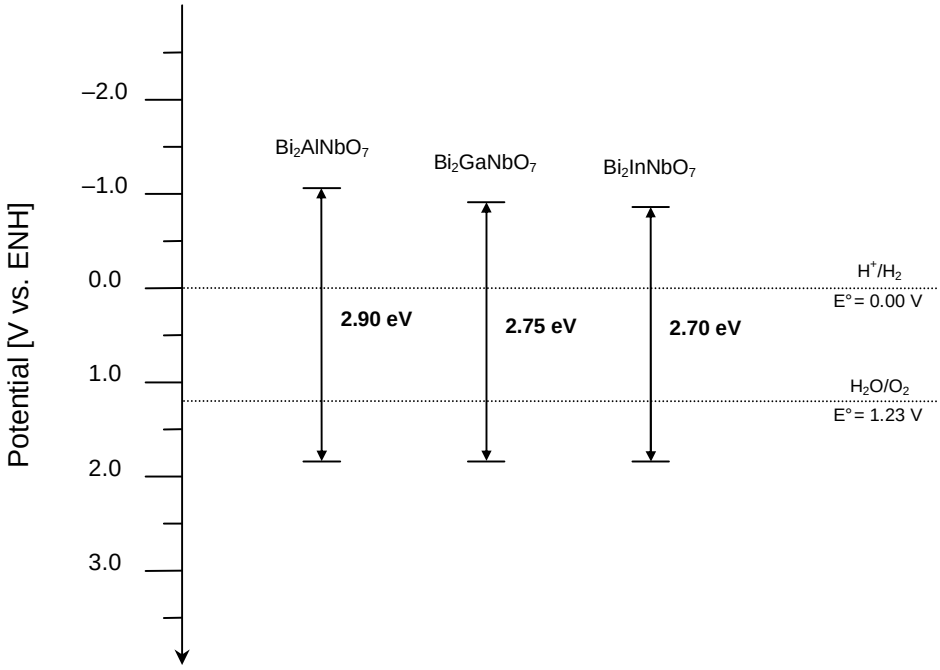

Figure 2. Diagram of bands materials Bi_2MNbO_7 (M = Al, In, Ga) to pH = 0.

In 2001, this family of semiconductors materials was for first time prepared through solid state reaction technique (SSR) [25]; using oxides and carbonates as raw material, which are submitted to high temperature (> 1000℃) and several conditions during a considerable time to allow the metal cations diffusion. However, this method generally leads to materials with low surface area (~1 m^2/g), non-uniform particle sizes and low purity of the crystalline phases. In 2006, Lorena L. Garza-Tovar et al [28] used the sol-gel method for the preparations of Bi_2MNbO_7 (M = Al, Fe, In, Sm) materials under soft conditions, where the structural and textural properties can be controlled. These materials were evaluated in methylene blue oxidation, showing an important increase of activity in regard to materials prepared by SSR.

On the other hand, it is necessary to support the semiconductors materials to make electrodes, since this form it allows to study their photoelectrochemical behavior and their use in photoassisted electrolysis of water. Also, the use of the supported materials allows increasing the useful life of the prepared material and it avoids the separation process of the powders after being used in suspension.

As support metal sheets can be used (stainless steel, aluminum, titanium) or conductor glass (ITO: *Indium-Tin Oxide*, FTO: *Fluorine-Tin Oxide*) which allow to obtain a transparent electrode with a larger area for the illumination [29].

The specific reactions that occur on the electrodes are dependent of the pH. In this work, the photoassisted electrolysis process was carried out to basic pH, for which the reactions can be represented by means of the following chemical equations:

$$2h^+ + 2OH^- \rightarrow {}^1/_2\, O_2 + H_2O \text{ (In the fotoanode)} \quad (1)$$

$$2e^- + 2H_2O \rightarrow H_2 + 2OH^- \text{ (In the catode)} \quad (2)$$

The use of sacrificial reducing agent (electron donors), as ethanol [30], methanol [31], Na_2SO_3, Na_2S, $Na_2S_2O_3$, $K_4[Fe(CN)_6]$, KI [32] and NaCN [33], has shown a considerable increase in the amount of hydrogen produced, because need an anodic reaction thermodynamically more favorable that increase the electron flow toward the cathode. In KCN case, which was used in this work, the reaction can be written as:

The use of sacrificial reducing agent (electron donors), as ethanol [30], methanol [31], Na_2SO_3, Na_2S, $Na_2S_2O_3$, $K_4[Fe(CN)_6]$, KI [32] and NaCN [33], has shown a considerable increase in the amount of hydrogen produced, because it implies an anodic reaction thermodynamically more favorable than increases the electrons flow toward the cathode. In the case of the KCN, which was used in this work, this reaction can be written as:

$$2h^+ + CN^- + 2OH^- \rightarrow CNO^- + H_2O \text{ (semiconductor)} \quad (3)$$

Keeping in mind the state of the art presented previously, this investigation project evaluated the performance of the materials Bi_2MNbO_7 (M= Al, Fe, Ga, In,)/SS pyrochlore type, prepared by sol-gel dip-coating method to be used as photoanodes in the hydrogen photoassisted production from water. In this process was evaluated the main operating variables as electrolyte concentration, the increase of solution conductivity and the presence of sacrificial reducing agents as KCN. As well as the influence of both the type of metal in the semiconductor structure and the type the cathodic material used in the electrochemical cell.

This report is divided in 5 chapters, through which it is present of order form the results obtained as product of the investigation.

In the first chapter, *Photocatalytic degradation of methyl orange using Bi_2MNbO_7 (M = Al, Fe, Ga, In) semiconductor films on stainless steel,* the photocatalytic activity of Bi_2MNbO_7 films was evaluated by the degradation of methyl orange and compared with the activity of TiO_2 films under the same reaction conditions. It was found that the photoactivity of Bi_2MNbO_7 films is higher or equivalent to TiO_2 films.

In the chapter 2, *Photoelectrochemical Hydrogen Production from Aqueous Solution Containing Cyanide Using Bi_2MNbO_7 (M = Al, Fe, Ga, In) Films on Stainless Steel as Photoanodes*, the preliminary results of photoelectrochemical hydrogen production are showed. In this process, the photoelectrocatalytic activity of materials of Bi_2MNbO_7 (M = Al, Fe, Ga, In) was compared in regard to TiO_2 under the same conditions. Furthermore, it is showed as electrolyte composition and concentration is a factor very important during the hydrogen generation.

In the chapter 3, *Photoelectrolytic hydrogen production using Bi_2MNbO_7 (M = Al, Ga) semiconductor film electrodes prepared by dip-coating*; the results as a function of the annealing temperature of photoanodes and electrolyte composition is showed; using the amount of hydrogen produced as response variable. It was found that the photoanodes evaluated has a very similar behavior, reaching your higher activity to annealing temperature of 500℃ in a electrolytic solution of 0.3 M of KOH and 120 ppm of CN^-.

El capítulo 4, *Photoelectrocatalytic hydrogen generation and cyanide oxidation using Bi_2MNbO_7 (M= In, Fe) films on stainless steel*, muestra una metodología muy similar a la presentada en el capítulo 3 con el objetivo de encontrar la composición del electrolito que permita obtener la mayor cantidad de hidrógeno posible. A diferencia de los resultados presentados en el capitulo dos, estos fotoánodos presentan diferencias significativas en su actividad photoelectrocatalítica, que pueden ser relacionadas con la carga superficial establecida por el pH de la solución electrolítica

The chapter 4, *Photoelectrocatalytic hydrogen generation and cyanide oxidation using Bi_2MNbO_7 (M= In, Fe) films on stainless steel*, a methodology very similar to the presented in the chapter 3 is showed with the objective of finding the electrolyte composition that allows to obtain the biggest quantity hydrogen. Contrary to the results presented in the chapter 2, these fotoanodes presents significant differences in their photoelectrocatalytic activity that can be related with the superficial load settled down by the pH of the electrolytic solution.

Finally in the chapter 5, *Hydrogen production by water splitting using Bi_2MNbO_7 (M = Al, Fe, Ga, In) films as photoanodes. A comparison between Ag, Pt and Pt/SS cathodes*, the evaluation of different cathodic materials in the production of hydrogen in search of to avoid the polarization of the silver cathode (employee in the previous chapters) due to the presence of the chloride of potassium is showed. In this chapter it was found that besides avoiding the polarization of the cathodic material, the highest values in current density and hydrogen production are obtained using the cathode of Pt/SS.

Bibliografía

[1] S. Ramesohl, F. Merten, Energy policy 34 (2006) 1251-1259.

[2] W. Lubitz, W. Tumas. Chem. Rev 107 (2007**)** 3900-3903.

[3] S.S. Penner, Energy 31 (2006) 33-43.

[4] Bak T, Nowotny J, Rekas M, Sorrell CC, Int J Hydrogen Energy 27 (2002) 991–1022.

[5] J. Nowotny, C.C. Sorrell, L.R. Sheppard, T. Bak. Int J Hydrogen Energy 30 (2005) 521 – 544.

[6] Hydrogen as an energy carrier. Royal Belgian Academy Council of Applied Science, April 2006.

[7] T.N. Veziroglou. Int J Hydrogen Energy 23 (1998) 1077–978.

[8] T.N. Veziroglou. Int J Hydrogen Energy 25 (2000) 1143–50.

[9] A. Fujishima, K. Honda. Nature 238 (1972) 37-38.

[10] J.O.M. Bockris, K. Uosaki, H. Kita. J Appl Phys 52 (1981) 808–810.

[11] H. Gerischer In: Seraphin BO, editor. Solar energy conversion. Amsterdam: Elsevier; 1979, p. 115–72.

[12] M. Grätzel, Artificial Photosynthesis: Water Cleavage into Hydrogen and Oxygen by Visible Light, Acc. Chem. Res. 14 (1981) 376.

[13] A. J. Bard, M.A. Fox, Acc. Chem. Res. 28 (1995) 141.

[14] M. Ni, M.K.H. Leung, D.Y.C. Leung, K. Sumathy, Renew. Sust Energy Rev. 11 (2007) 401-425.

[15] A. Fujishima, K. Honda, Bull Chem Soc Jpn 44 (1971) 1148.

[16] A. Fujishima, K. Kohayakawa, K. Honda, J Electrochem Soc 122 (1975) 487.

[17] A.L. Linsebigler, G. Lu, J. T. Jr Yates. Chem Rev 95 (1995) 735.

[18] A. Fujishima, T.N. Rao, D.A. Tryk. J Photochem Photobiol C

Photochem Rev 1 (2000) 1.

[19] O. Carp, C.L. Huisman, A. Reller. Prog Solid State Chem 32 (2004) 33.

[20] J. Rodríguez J, R.J. Candal, J. Solís, W. Estrada, M.A. Blesa. (2005) In: M.A. Blesa, J. Blanco Gálvez (eds) Solar safe water: tecnologías solares para la desinfección y descontaminación del agua, chapter 9. Escuela de Posgrado UNSAM, San Martín.

[21] K. Hashimoto, H. Irie, A. Fujishima. Jpn J Appl Phys 44 (2005) 8269.

[22] J. Rodríguez, R.J. Candal, J. Solís, W. Estrada, M.A. Blesa, El fotocatalizador: síntesis, propiedades y limitaciones, en: M.A. Blesa, J. Blanco (Eds.), Solar Safe Water: Tecnologías solares para la desinfección y descontaminación del agua, ByToner, La Plata (Argentina), 2005. Cap. 9, p. 129-146.

[23] P.V. Kamat. Chem. Rev. 93 (1993) 267-300.

[24] A. Nemecsics, S. Kovács, Z. Lábadi, K.F. Hesse, M. Czank, P. Turmezei, S. Motrya (2005) *Sol. Energy Mater. Sol. Cells* 89:175.

[25] Z. Zou, J. Ye, H. Arakawa. Solid State Commun. 116 (2000) 259-263.

[26] Z. Zou, J. Ye, H. Arakawa. Int. J. Hydrogen Energy 28 (2003) 663–669.

[27] Z. Zou, J. Ye, H. Arakawa. Chem. Phys. Lett. 333 (2001) 57-62.

[28] L.L. Garza-Tovar, Leticia M. Torres-Martínez, D. Bernal Rodríguez, R. Gómez, y G. del Ángel. J. Mol. Catal. A: Chem. 247 (2006) 283-290.

[29] Q. Qiao, J. Beck, R. Lumpkin, J. Pretko, James T. Mcleskey, Jr. Sol. Energy Mater. Sol. Cells 90 (2006) 1034-1040.

[30] G.R. Bamwenda, S. Tsubota, T. Nakamura, M. Haruta, Photoassisted hydrogen production from a water-ethanol solution: a comparison of activities of Au-TiO_2 and Pt-TiO_2, J. Photochem. Photobiol. A: Chem. 89 (1995) 177-189.

[31] N.L. Wu, M.S. Lee, Z.J. Pon, J.Z. Hsu. J. Photochem. Photobiol. A: Chem. 163 (2004) 277-280.

[32]T. Ohmori, H. Mametsuka, E. Suzuki, Photocatalytic hydrogen evolution on InP suspension with inorganic sacrificial reducing agent, Int. J. Hydrogen Energy 25 (2000) 953-955.

[33] S.G. Lee, S. Lee, H.I. Lee. Appl. Catal. A: General 207 (2001) 173-181.

CHAPTER 1.

Photocatalytic degradation of methyl orange using Bi_2MNbO_7 (M = Al, Fe, Ga, In) semiconductor films on stainless steel

Abstract

Semiconductor Bi_2MNbO_7 (M = Al, Fe, Ga, In) films were prepared by sol-gel method. The films were deposited on AISI-SAE 304 stainless steel at three different withdrawal speeds using the dip-coating technique and annealed at 500 ºC. Films were characterized by X-Ray Diffraction, Scanning Electron Microscopy and X-Ray Fluorescence Spectroscopy. The photocatalytic activity of Bi_2MNbO_7 films was evaluated by the degradation of methyl orange and compared with the activity of TiO_2 films under the same reaction conditions. Films exhibited the following photocatalytic performance: Bi_2GaNbO_7 > Bi_2FeNbO_7 > Bi_2AlNbO_7 > TiO_2 ≥ Bi_2InNbO_7 >> UV light. It is worth noting that the Bi_2MNbO_7 films have results as good as titanium dioxide in the degradation of methyl orange. Furthermore, the kinetic of the photodegradation of the methyl orange has been investigated.

1.1 Introduction

Recently, the so-called Advanced Oxidation Processes (AOPs) have been proposed as alternative methods for water purification [1,2]. Among AOPs, heterogeneous photocatalysis appears as an emerging destructive technology leading to the total mineralization of most of the organic pollutants [3-5]. Titanium dioxide suspension has been extensively used for water treatment and other process due to its exceptional optical and electronic properties, chemical stability, non-toxicity and low cost [6-8]. One of the disadvantages of using TiO_2 in these processes is the need to illuminate them with high-energy photons (UV light). For this reason, the search for new promising photocatalysts that can operate with visible light is an important challenge to extend the range of their applications [9,10]. In this sense, a series of photo-catalysts that can extend their response to UV-Vis, have been synthesized and tested in the photo-catalytic hydrogen production [11,12] and photo-degradation of methylene blue [13], showing a high

activity, when materials suspensions are used, these must be recovered at the end of the treatment, either by filtration or sedimentation which is expensive in terms of time, reagents and manpower [14]. The immobilization, in the form a film, of the catalyst on inert support surfaces has been recently used in order to avoid the catalyst-recovering step [15-17]. In present study, photodegradation of methyl orange (MeO, Fig. 1.1), used as a model molecule, was studied using as photocatalyst Bi_2MNbO_7 semiconductor films prepared by sol-gel method and supported on AISI-SAE 304 stainless steel by dip-coating technique.

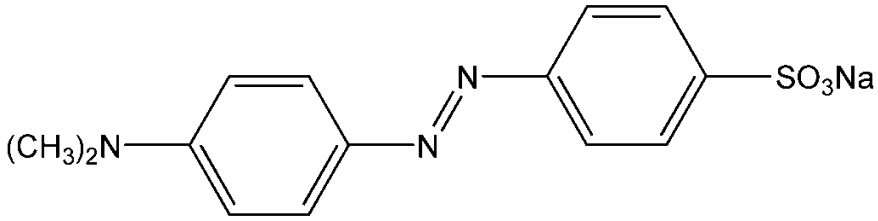

Fig. 1.1. Molecular structure of MeO.

1.2. Experimental

1.2.1. Materials

The following reagents were used as received without further purification: bismuth(III) acetate (Aldrich, 99.99%), aluminum(III) acetylacetonate (Aldrich, 99.999%), gallium(III) acetylacetonate (Aldrich, 99.99%), indium(III) acetylacetonate (Aldrich, 99.99%), iron(III) acetylacetonate (Aldrich, 99.9%), niobium(V) ethoxide (Aldrich, 99.95%), titanium(IV) isopropoxide (Aldrich, 97%), 2-propanol (Merck, 99,5%), ethanol (Merck, 99.9%), acetylacetone (Aldrich, 99%), HNO_3 (Carlo Erba, 65%), methyl orange (Merck, 100%) and distilled water (1 MΩ·cm).

1.2.2. Preparation of the films

Semiconductor films of Bi-M-Nb-O (M = Al, Fe, Ga, In) were prepared by dip-coating on AISI/SAE 304 stainless steel (304 SS) plates (15 mm x 25 mm), which were ultrasonically cleaned in ethanol (15 min) prior to use. Details of the sol preparation were described elsewhere [15]. Briefly, films of Bi–M–Nb–O (M= Al, Ga, In, Fe) system were prepared by dissolving the corresponding metal (M) precursor in a solution of ethanol:HNO_3:acac:water. The solution was kept under constant agitation for 15 min. Then stoichiometric amounts of bismuth(III) acetate in ethanol:HNO3:acac and niobium(V) ethoxide in ethanol:acac were added dropwise to the initial solution. The resulting suspension was kept in constant agitation during 24 h at 25 ℃ until the sol was fo rmed. The films were made at different withdrawal speeds (5.0, 7.5 and 10.0 cm/min) with different number of

layers (1, 3 and 5). The films were dried at room temperature (25℃) for 1 h after each layer deposition. Finally, they were annealed at 500℃ for 4 h.

TiO_2 films were also prepared by similar procedure for comparative purposes [18].

1.2.3. Characterization of the films

Scanning electron microscopy (SEM) micrographs were obtained with a LEO 430 microscope operated at 20 kV in secondary electron mode.

X-ray diffraction (XRD) patterns were collected on a PANalytical X'Pert PRO diffractometer operated at 40 kV and 40 mA, using Cu Kα radiation (λ = 1.540598 Å) selected with Ni filter, in the thin film mode with a step of 0.02° and a counting time of 1.0 s per step.

Elemental analyses were performed by energy dispersive X-ray fluorescence (EDXRF) in a Shimadzu EDX-800HS spectrometer equipped with a Rh tube and a Si(Li) detector. The measurements were performed in vacuum atmosphere and the quantification was performed using fundamental parameters method.

1.2.4. Photocatalytic evaluation of the films

Photocatalytic activity of the Bi_2MNbO_7 (M = Al, Fe, Ga, In) films deposited on AISI/SAE 304 stainless steel support was evaluated on the degradation of methyl orange (MeO), used as model molecule [19-21]. A 200 mL glass cell equipped with an immersion Hg lamp (UVP Pen-Ray 5.5 W) was employed in the photocatalytic experiments (Fig. 1.2). In all tests, 40 mL of aqueous solution containing 5 ppm of MeO were used at natural pH. Before starting each test, the system was kept in the dark for 15 min to achieve the adsorption equilibrium. The reaction was carried out during 2 h with continuous air bubbling and magnetic stirring. Samples were taken each 30 min and the MeO concentration was determined by colorimetry, using the 460 nm absorption band, in a LaMotte Smart apparatus. The reaction was also carried out using TiO_2 films deposited on AISI/SAE 304 stainless steel as reference. Blank reaction was done without semiconductor films in order to determine the contribution of photolytic degradation.

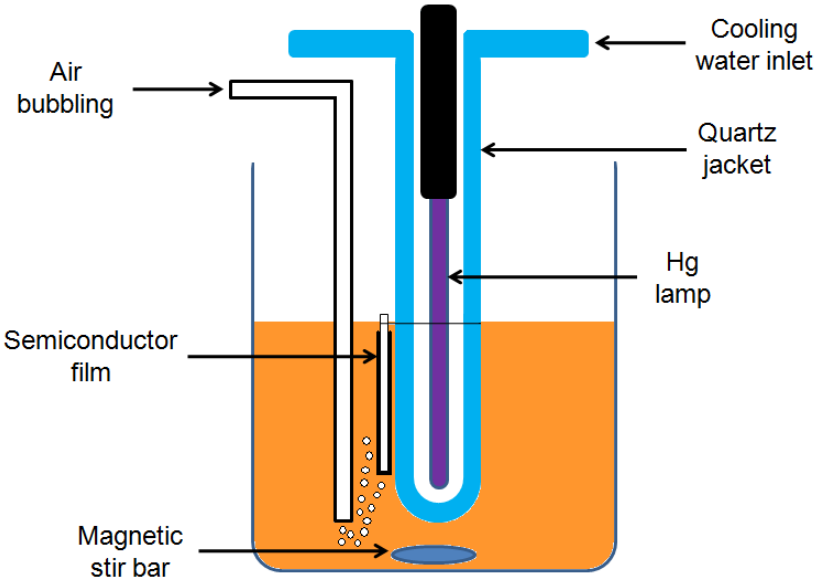

Fig. 1.2. Schematic representation of the photoreactor.

1.3 Results and discussion

1.3.1. Scanning electron microscopy

SEM micrograph of Bi_2GaNbO_7 film (1 layer) on 304 SS obtained at 5.0 cm/min show a fairly flat but cracked surface (Fig. 1.3a). The formation of microcracks all over the surface may be a consequence of the coating contraction during the heat treatment [22]. When the withdrawal speed was increased to 7.5 cm/min, the cracks became slightly thinner (Fig. 1.3b) probably because the thickness of the films increased.

When the number of deposited layers was increased to 3, the cracks were covered partially but agglomerates appeared (Figs. 1.3c and 1.3d) because the amount of deposited material increased.

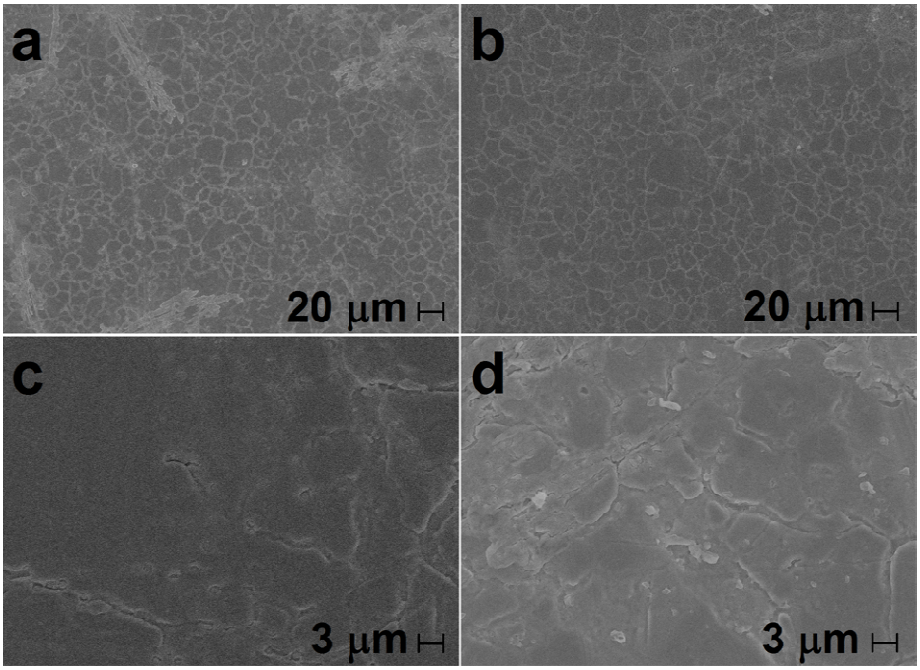

Fig. 1.3. SEM micrographs of Bi_2GaNbO_7 films on 304 SS: (a) 1 layer at 5.0 cm/min (1000x), (b) 1 layer at 7.5 cm/min (1000x), (c) 3 layers at 5.0 cm/min (7000x), (d) 3 layers at 7.5 cm/min (7000x).

1.3.2. X-ray diffraction

XRD patterns of Bi_2MNbO_7 (M = Al, Fe, Ga, In) films on 304 SS (3 layers at 7.5 cm/min) are shown in Fig. 1.4.

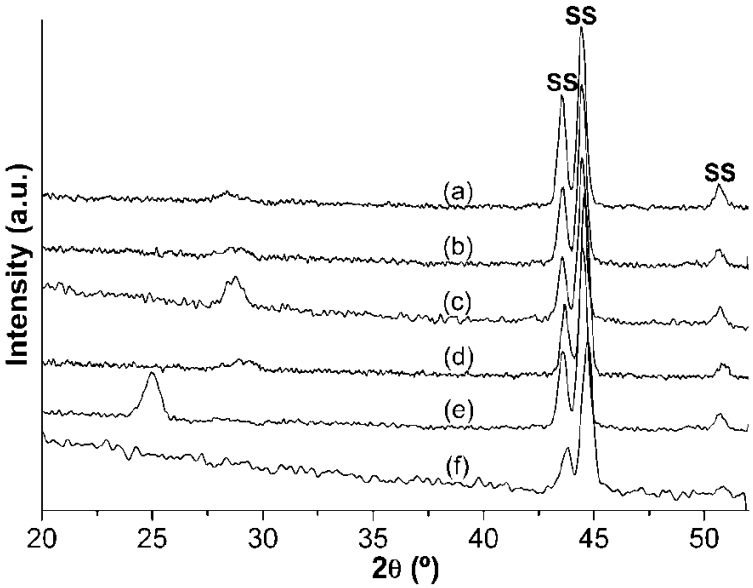

Fig. 1.4 XRD patterns of (a) Bi_2AlNbO_7, (b) Bi_2FeNbO_7, (c) Bi_2GaNbO_7, (d) Bi_2InNbO_7 and (e) TiO_2 films on 304 SS (3 layers at 7.5 cm/min) and (f) 304 SS annealed at 500℃.

In the XRD patterns of the sol-gel Bi_2MNbO_7 (M = Al, Fe, Ga, In) films, only broads peaks at about 28.7º corresponding to the pyrochlore structure-type could be identified [23]. The peaks present at 43.6, 44.6 and 50.7º correspond to the stainless steel support [24]. It is strongly proposed that such a broad peaks are due the small crystallite size and the poor crystallinity [25]. Although the Bi_2MNbO_7 films showed similar XRD patterns, the 2θ angles of the pyrochlore reflection were slightly different: Bi_2AlNbO_7 (28.37º) < Bi_2FeNbO_7 (28.63º) < Bi_2GaNbO_7 (28.77º) < Bi_2InNbO_7 (28.97º). They were shifted according to the ionic radius of the 6-coordinated substituent atom M^{3+}: Al (67.5 pm) < Fe (69 pm) < Ga (76 pm) < In (94 pm) [26]. It is worth noting that the (101) anatase reflection at 2θ=25.11 in the XRD pattern of the TiO_2 film (Fig. 1.4e) is more intense that the corresponding pyrochlore reflections indicating that this material has more crystallinity that the corresponding ones.

1.3.3 Energy dispersive X-ray fluorescence

EDXRF results, showed in table 1.1, indicate that the elemental proportion in Bi-Ga-Nb-O sample fits better to the stoichiometric ratio (Bi:Ga:Nb = 2:1:1) of pyrochlore-type structure (Bi_2GaNbO_7). In the other samples a Bi excess was detected suggesting the presence of $Bi_5Nb_3O_{15}$ [27], $Bi_5In_2Nb_3O_{18-x}$ [28] or Bi_2O_3/Bi_2O_{4-x} [29].

Table 1.1. Elemental analyses of Bi_2MNbO_7 (M = Al, Fe, Ga, In) films (3 layers at 7.5 cm/min) on 304 SS are summarized in Table 1.1

Film	Bi (at. %)	M (at. %)	Nb (at. %)
Bi_2AlNbO_7	70.3	16.1	13.6
Bi_2FeNbO_7	64.8	19.1	16.1
Bi_2GaNbO_7	54.5	23.1	22.4
Bi_2InNbO_7	76.7	12.6	10.7
Bi_2MNbO_7[a]	50.0	25.0	25.0

[a] Stoichiometric ratio.

1.3.5. Photodegradation of methyl orange

MeO degradation over time using Bi_2MNbO_7 (M = Al, Fe, Ga, In) and TiO_2 films on 304 SS (3 layers at 7.5 cm/min) is shown in Fig. 1.5.

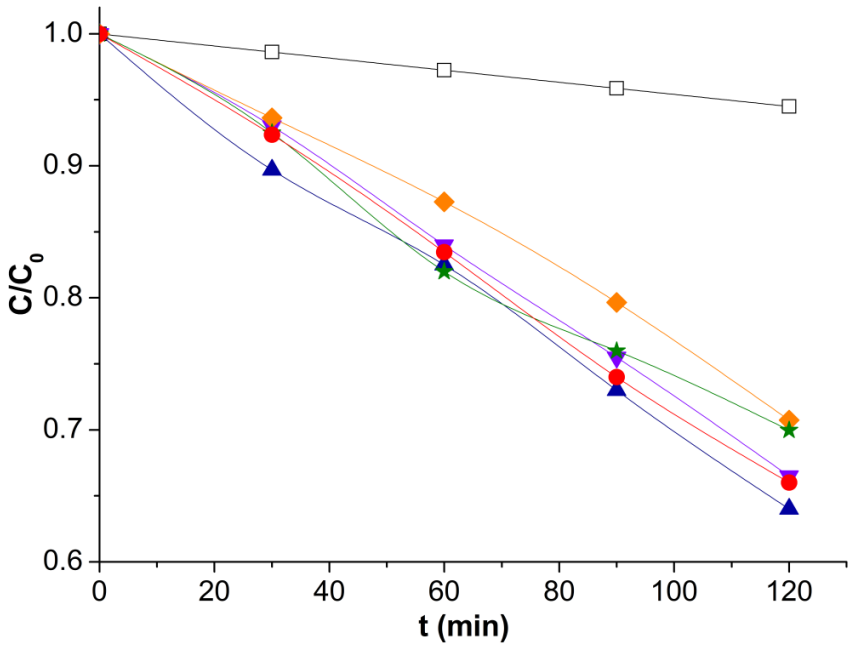

Fig. 1.5 Relative concentration of MeO vs. time using: (▼) Bi_2AlNbO_7, (●) Bi_2FeNbO_7, (▲) Bi_2GaNbO_7, (◆) Bi_2InNbO_7 and (★) TiO2 films on 304 SS (3 layers at 7.5 cm/min) and (☐) UV light (without photocatalyst).

In Fig. 1.5 it can be seen that the films exhibit the following photocatalytic performance: Bi_2GaNbO_7 > Bi_2FeNbO_7 > Bi_2AlNbO_7 > TiO_2 ≥ Bi_2InNbO_7 >> UV light. Slight differences between the films with different substituent atom M were detected. These can be correlated to their stoichiometric deviations in regard to Bi_2MNbO_7 (see Table 1.1). Although the photoactivity of Bi_2InNbO_7 is comparable to that of TiO_2 at the end of the test, it is worth noting that the second one decreases with the time. There is a change in the slope at about 60 min. The photocatalytic behavior of Bi_2MNbO_7 (M = Al, Fe, Ga, In) with regard to TiO_2 films could be related to their poor crystallinity (see Fig. 1.4).

The curves C/C_0 vs. time are well described by a mono-exponential curve suggesting that a pseudo-first-order reaction model can be used to describe the kinetic behavior of the films. Using a modified Langmuir-Hinshelwood model, the rate of photodegradation can be expressed as:

$$r = -\frac{dC}{dt} = \frac{k_r K C_0}{1 + K C_0} \tag{1}$$

Due to the low concentration of methyl orange ($KC_0 << 1$), the term KC_0 in the denominator could be neglected. Integration of Eq. (1) with initial condition $C = C_0$ at $t = 0$ gives:

$$\ln\left(\frac{C_0}{C}\right) = k_{app} t \tag{2}$$

where $k_{app} = k_r K$ is an apparent first-order rate constant.

The plot of $\ln C_0/C$ vs. t represents a straight line and is shown in Fig. 1.6. The slope of linear regression is k_{app}.

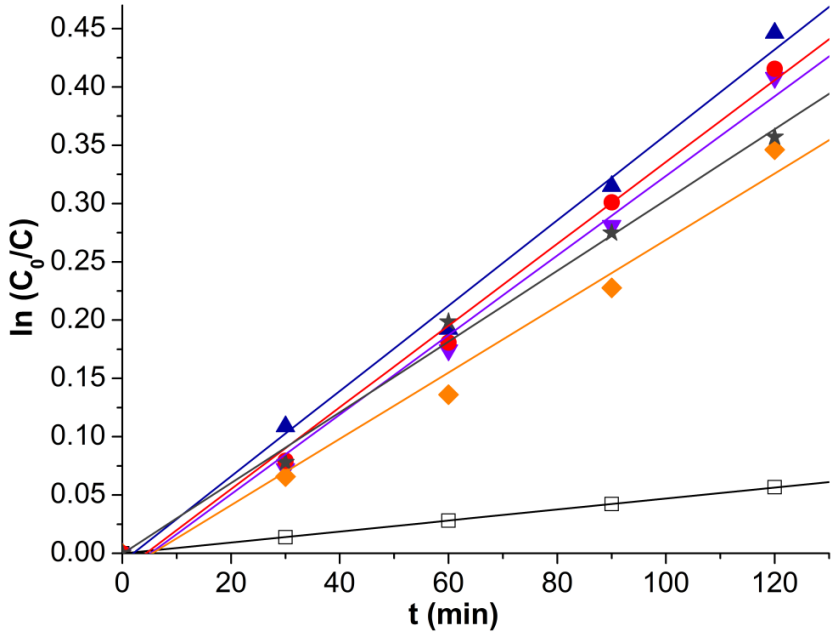

Fig. 1.6 Linear transformation of the relative concentration of MeO vs. time using: (▼) Bi_2AlNbO_7, (●) Bi_2FeNbO_7, (▲) Bi_2GaNbO_7, (◆) Bi_2InNbO_7 and (★) TiO2 films on 304 SS (3 layers at 7.5 cm/min) and (☐) UV light (without photocatalyst).

For a pseudo-first-order reaction, the half-life time ($t_{1/2}$) can be calculated according Eq. 3:

$$t_{1/2} = \frac{\ln 2}{k_{app}} \qquad (3)$$

The corresponding values of the kinetic parameters (k_{app}, $t_{1/2}$) for each photocatalyst are shown in Table .12.

All the films showed a higher photocatalytic activity than those obtained only with UV light. The photoactivity of Bi_2MNbO_7 films was higher or equivalent than TiO_2 films. The Bi_2GaNbO_7 film exhibited the highest k_{app} and therefore the lowest $t_{1/2}$. This result can be explained due to the Bi-Ga-Nb-O system fits better to the stoichiometric ratio in Bi_2MNbO_7 according to the EDXRF results (see Table 1.1).

Table 1.2 Kinetic parameters for the MeO photodegradation (2 h) over Bi_2MNbO_7 (M = Al, Fe, Ga, In) films on 304 SS (3 layers at 7.5 cm/min).

Photocatalyst	Apparent first-order rate constant, $k_{app} \times 10^{-3}$ (min^{-1})	Half-life time, $t_{1/2}$ (min)	Correlation coefficient, R^2
UV light	0.47	1475	0.9999
Bi_2AlNbO_7	3.41	203	0.9955
Bi_2FeNbO_7	3.51	197	0.9971
Bi_2GaNbO_7	3.66	189	0.9969
Bi_2InNbO_7	2.85	243	0.9919
TiO_2	3.04	228	0.9970

MeO degradation over time using Bi_2GaNbO_7 films on 304 SS (3 layers) made at different withdrawal speed (5.0, 7.5 and 10.0 cm/min) is shown in Fig. 1.7

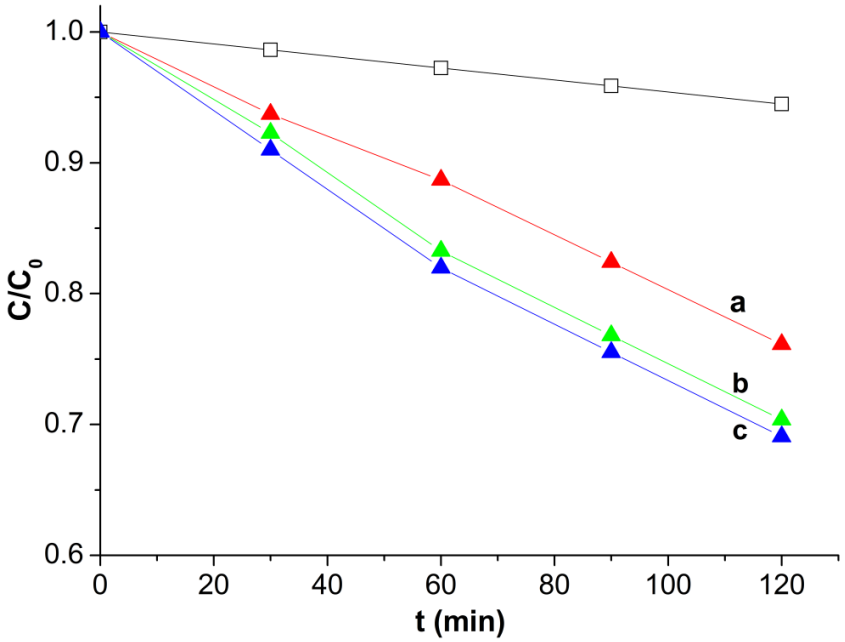

Fig. 1.7 Relative concentration of MeO vs. time using (▲) Bi_2GaNbO_7 films (3 layers) made at a withdrawal speed of: (a) 5.0 cm/min, (b) 7.5 cm/min, (c) 10.0 cm/min and (☐) UV light (without photocatalyst).

In Fig. 1.7 it can be seen that the degradation increases with a faster withdrawal speed. The highest degradation was achieved with the films made at the fastest withdrawal speed (10.0 cm/min). This behavior can be explained by the higher amount of deposited material when a faster withdrawal speed was used, according to the equation proposed by Landau and Levich, which expresses that the film thickness is directly proportional to the withdrawal speed [30,31]. However, it is worth noting that a significant difference in the degradation was not detected when the withdrawal speed was increased from 7.5 to 10.0 cm/min. This result could be due to two factors: (1) further increments in the withdrawal speed after certain value not lead to an increase in the thickness or (2) further increments in the amount of deposited material after certain value are not followed by an increase in the degradation. It is worth mentioning that similar results in the photodegradation behavior were obtained using Bi_2GaNbO_7 films on 304 SS (1 layer) made at the same withdrawal speeds and therefore the previous result could be attributed mainly to the first factor.

MeO degradation over time using Bi_2GaNbO_7 films on 304 SS with different number of layers (1, 3 and 5) at a withdrawal speed of 7.5 cm/min is shown in Fig. 1.8.

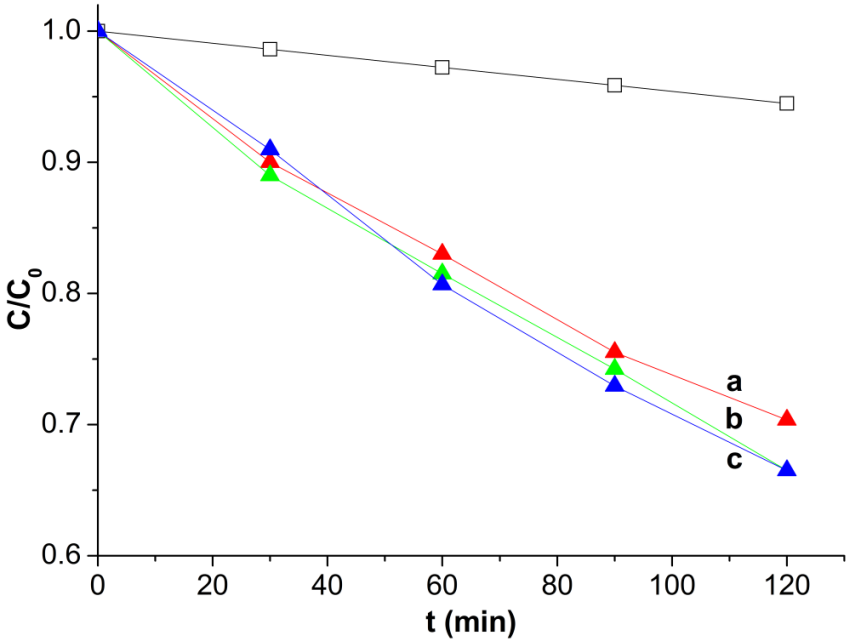

Fig. 1.8 Relative concentration of MeO vs. time using (▲) Bi_2GaNbO_7 films with different number of layers (7.5 cm/min): (a) 1, (b) 3, (c) 5 and (□) UV light (without photocatalyst).

In Fig. 1.8 it can be seen that the degradation increases when the number of layers was increased from 1 to 3 but a further increment to 5 layers not lead to any

improvement. Undoubtedly, the enhancement in the degradation until a certain value is due to the increase in the amount of deposited material with the augment of number of layers. It is worth mentioning that the behavior of the other films was similar.

All materials used in the photo-degradation of MeO were subjected to several cycles of use, among which there were no significant changes in their photocatalytic performance, showing stability and resistance to the reaction conditions employed. The obtained results with the sol-gel method and dip-coating technique make further work on the subject very encouraging.

1.4 Conclusions

The photoactivity of Bi_2MNbO_7 films was higher or equivalent to TiO_2 films. The Bi_2GaNbO_7 film has the major cristallinity and the best elemental proportion according to pyrochlore-type structure, exhibiting the major photocatalytic activity and the highest k_{app} and therefore the lowest $t_{1/2}$.

The photodegradation of MeO increase with a faster withdrawal speed and with increases of the number of layer deposited. Degradation of MeO follows an apparent first order kinetics as most of the pollutant, which confirm the heterogeneous catalytic character of system for diluted solution.

1.5 References

[1] T. Oppenländer, Photochemical Purification of Water and Air. Advanced Oxidation Processes (AOPs): Principles, Reaction Mechanisms, Reactor Concepts, Wiley VCH, Weinheim, 2003.

[2] S. Parsons, Advanced Oxidation Processes for Water and Wastewater Treatment, IWA Publishing, London, 2004.

[3] I.K. Konstantinou, T.A. Albanis, Appl. Catal. B: Environ., 49 (2004) 1.

[4] U.I. Gaya, A.H. Abdullah, J. Photochem. Photobiol. C: Photochem. Rev. 9 (2008) 1.

[5] K. Rajeshwar, M.E. Osugi, W. Chanmanee, C.R. Chenthamarakshan, M.V.B. Zanoni, P. Kajitvichyanukul, R. Krishnan-Ayer, J. Photochem. Photobiol. C: Photochem. Rev. 9 (2008) 171,

[6] A.G. Agrios, P. Pichat, J. Appl. Electrochem. 35 (2005) 655.

[7] A. Fujishima, X. Zhang, C. R. Chimie 9 (2006) 750.

[8] M. Kitano, M. Matsuoka, M. Ueshima, M. Anpo, Appl. Catal. A: General 325 (2007) 1.

[9] K. Sayama, K. Yase, H. Arakawa, K. Asakura, K. Tanaka, K. Domen, T.J. Onishi, J. Photochem. Photobiol. A: Chem. 114 (1998) 125.

[10] M. Anpo, M. Takeuchi, J. Catal. 216 (2003) 505.

[11] Z. Zou, J. Ye, H. Arakawa, J. Mol. Catal. A: Chem. 168 (2001) 289.

[12] Z. Zou, H. Arakawa, J. Photochem. Photobiol. A: Chem. 158 (2003) 145.

[13] L.L. Garza-Tovar, L.M. Torres-Martínez, D. Bernal Rodríguez, R. Gómez, G. del Angel, J. Mol. Catal. A Chem. 247 (2006) 283.

[14] J.M. Herrmann, J. Disdier, P. Pichat, S. Malato, J. Blanco, Appl. Catal. B: Environ. 17 (1998) 15.

[15] J.L. Ropero-Vega, K.L. Rosas-Barrera, J.A. Pedraza-Avella, D. Laverde-Cataño, J.E. Pedraza-Rosas, M.E. Niño-Gómez, Mater. Sci. Eng. B 174 (2010) 196–199

[16] H.M. Coleman, B.R. Eggins, J.A. Byrne, F.L. Palmer, E. King, Appl. Catal. B: Environ. 24 (2000) L1.

[17] H.T. Chang, N. Wu, F. Zhu, Water Res. 34 (2000) 407.

[18] K.H. Yoon, J.S. Noh, C.H. Kwon, M. Muhammed, Mater. Chem. Phys. 95 (2006) 79.

[19] G.T. Brown, J.R. Darwent, J. Phys. Chem. 88 (1984) 4955.

[20] I.M. Arabatzis, T. Stergiopoulos, M.C. Bernard, D. Labou, S.G. Neophytides, P. Falaras, Appl. Catal. B: Environ. 42 (2003) 187.

[21] Z. Zainal, L.K. Hui, M.Z. Hussein, Y.H. Taufiq-Yap, A.H. Abdullah, I. Ramli, J. Hazard. Mater. 125 (2005) 113.

[22] G. Balasubramanian, D.D. Dionysiou, M.T. Suidan, J. Mater. Sci. 38 (2003) 823.

[23] Z. Zou, J. Ye, H. Arakawa, Mater. Sci. Eng. B 79 (2001) 83.

[24] S. Sokolov, E. Ortel, J. Radnik, R. Kraehnert, Thin Solid Films 518 (2009) 27.

[25] I.M. Arabatzis, S. Antonaraki, T. Stergiopoulos, A. Hiskia, E. Papaconstantinou, M.C. Bernard, P. Falaras, J. Photochem. Photobiol. A: Chem. 149 (2002) 237.

[26] J.E. Huheey, E.A. Keiter, R.L. Keiter, Química Inorgánica: Principios de estructura y reactividad, 4th ed., Oxford University Press, México, 1997. p. 120.

[27] L.L. Garza-Tovar, L.M. Torres-Martínez, D. Bernal Rodríguez, R. Gómez, G. del Angel, J. Mol. Catal. A: Chem. 247 (2006) 283.

[28] Z. Zou, J. Ye, J. Alloys Compd. 292 (1999) 72.

[29] A. Hameed, T. Montini, V. Gombac, P. Fornasiero, J. Am. Chem. Soc. 130 (2008) 9658.

[30] C.J. Brinker, G.W. Scherer, Sol-Gel Science: The Physics and the Chemistry of Sol-Gel Processing, Academic Press INC, San Diego, 1990, p. 790.

[31] R.J. Candal, J. Rodriguez, G. Colón, S. Gelover, E. Vigil Santos, A. Jimenez González, M.A. Blesa, Materiales para fotocatálisis y electrofotocatálisis, in: M.A. Blesa, B. Sánchez (Eds.), Eliminación de contaminantes por fotocatálisis heterogénea, CIEMAT, Madrid, 2004, p. 189.

CHAPTER 2.

Photoelectrochemical Hydrogen Production from Aqueous Solution Containing Cyanide Using Bi_2MNbO_7 (M = Al, Fe, Ga, In) Films on Stainless Steel as Photoanodes

Abstract

Photoelectrochemical water splitting (UV-Vis, 2.5 V) from alkaline solution containing cyanide was evaluated in a conventional two-compartment electrochemical cell using Bi_2MNbO_7 (M = Al, Fe, Ga, In) films on AISI/SAE 304 stainless steel as photoanode and a silver plate as cathode. The films were prepared by sol-gel dip-coating followed by a thermal treatment at 500 ℃. They were characterized by scanning electron microscopy, X-ray diffraction and energy dispersive X-ray fluorescence. During the photoelectrochemical process, both circulating current and hydrogen production were measured. Changes in cyanide concentration were determined by potentiometric titration. The activity of Bi_2MNbO_7 films was higher or equivalent to that of TiO_2 film and dependent on the electrolyte composition and concentration. The obtained results make further work on the subject very encouraging.

2.1 Introduction

Since the pioneering works of Fujishima & Honda [1-3] and Frank & Bard [4-6] photoelectrochemistry and semiconductor photocatalysis for hydrogen production and environmental cleanup have attracted a great interest because of their potential in solar energy conversion [7-11].

Initial interest in these photoinduced reactions was prompted by the discovery that water could be split (simultaneously oxidized and reduced to form O_2 and H_2, respectively) in a photoelectrochemical cell upon illuminating a TiO_2-single crystal photoanode and having an inert cathode to which a small electrochemical bias had been applied [1-3]. It soon became apparent that novel redox reactions of inorganic compounds, such as CN^- and SO_3^{2-}, and other organic compounds could also be induced by band-gap irradiation of a variety of

semiconductor particles [4, 6]. More focused scientific interest in these reactions has also developed within the last decade due to the suggested use of photoexcited TiO_2 dispersions in environmental protection and amelioration [12-16]. Since then, research efforts to understand the fundamental processes and to enhance the photocatalytic efficiency of TiO_2 have come from extensive work performed by chemists, physicists and chemical engineerings [17-21]. Nowadays, a growing interest in hydrogen generation (as a combustible fuel), using solar energy and renewable sources such as water, has focused the attention again on the photoelectrochemical water splitting [22-26].

Historically, TiO_2 is the material which really sparked interest in the photoelectrolysis of water [1-3]. However, from the viewpoint of H_2 production, it is not very attractive due to the position of its conduction band edge with respect to the redox potential of H_2/H_2O couple and its low visible light absorption [27-31].

Current research is focused on the modification of TiO_2 [32-36] as well as the development of new semiconductor materials, such as titanates, vanadates niobates and tantalates [37-41]. Other groups investigate the use of sacrificial reducing agents or electron donors [42-46], which can also be present in water as unwanted species like CN^- [4-6, 42, 47-52].

In this work, we evaluated for the first time the photoelectrochemical H_2 production from aqueous solution containing CN^- by using Bi_2MNbO_7 (M = Al, Fe, Ga, In) films on stainless steel as photoanode. This new series of promising photocatalysts for water decomposition with visible light was first synthesized as powders, by a solid-state reaction [53-57] and a sol-gel process [58], and recently as thin films, by sol-gel dip-coating [59-61].

2.2 Experimental

2.2.1. Materials

The following reagents were used as received without further purification: bismuth(III) acetate (Aldrich, 99.99%), aluminum(III) acetylacetonate (Aldrich, 99.999%), gallium(III) acetylacetonate (Aldrich, 99.99%), indium(III) acetylacetonate (Aldrich, 99.99%), iron(III) acetylacetonate (Aldrich, 99.9%), niobium(V) ethoxide (Aldrich, 99.95%), ethanol (Merck, 99.9%), acetylacetone (Aldrich, 99%), HNO_3 (Carlo Erba, 65%), titanium(IV) isopropoxide (Aldrich, 97%), 2-propanol (Merck, 99.5%), KOH (Carlo Erba, 85%), KCN (Aldrich, 97%), KCl (Merck, 99.5%), $AgNO_3$ (Carlo Erba, ACS-ISO for analysis), NaCl (Merck, 99.5%) and distilled water (1 MΩ·cm).

2.2.2. Preparation of the films

Semiconductor films of Bi-M-Nb-O (M = Al, Fe, Ga, In) system were prepared by sol-gel dip-coating on AISI/SAE 304 stainless steel (304 SS) plates. Briefly, an alcoholic suspension was made by mixing stoichiometric amounts of the corresponding metal precursors (the reagents mentioned above), in the presence of a complexing agent (acetylacetone). Details of the preparation have been described elsewhere [59]. Subsequently, by hydrolysis and polycondensation reactions, a stable sol was formed and used for the preparation of films on metallic substrates (15 mm × 25 mm), which were degreased by sonication in ethanol (15 min) and rinsed with distilled water. The films were made at a withdrawal speed of 7.5 cm/min. They were dried at room temperature (25℃) for 20 min and finally annealed in air at 500℃ for 4 h.

TiO_2 film was also prepared by a similar procedure for comparative purposes [62].

2.2.3. Characterization of the films

Scanning electron microscopy (SEM) images were obtained with a LEO 430 microscope operated at 20 kV in secondary electron mode.

X-ray diffraction (XRD) patterns were collected on a PANalytical X'Pert PRO diffractometer operated at 40 kV and 40 mA, using Cu Kα radiation (λ = 1.540598 Å) selected with Ni filter, in the thin film mode with a step of 0.02° and a counting time of 1.0 s per step.

Elemental analyses were performed by energy dispersive X-ray fluorescence (EDXRF) in a Shimadzu EDX-800HS spectrometer equipped with a Rh tube and a Si(Li) detector. The measurements were done in vacuum atmosphere and the quantification was performed using fundamental parameter method.

2.2.4. Photoelectrochemical evaluation of the films

The performance of the prepared films was tested in photoelectrocatalytic water splitting from alkaline solutions (0.1-0.3 M KOH) containing cyanide as sacrificial reducing agent (100-300 ppm CN^-), in resemblance to gold mining effluents. The experiments was conducted in a conventional cell with two cylindrical compartments (D = 4 cm, h = 4 cm) separated by an anion exchange membrane (Ameridia Neosepta AMX), see Fig. 3.1. The prepared films were used as photoanode and a silver plate (15 mm × 25 mm) was used as cathode. They were separated by 2 cm and connected with a copper wire to a DC power supply

(Hewlett Packard 6282A) operating at 2.5 V. Outer-irradiation was provided by a high pressure mercury-lamp (General Electric Kolorlux, 125 W). The circulating current and potential differences applied on the electrodes were measured at least every 10 min during 1 to 3 h with an Amprobe 30XR-A digital multimeter. The hydrogen concentration in the headspace of the cathodic compartment (15 mL) was measured each 30 min during 1 to 3 h with a Crowcon Tetra gas analyzer (detection range: 0-1000 ppm, detection limit: 1 ppm). Finally, changes in the cyanide concentration in the anodic compartment (35 mL) were determined by potentiometric titration on a Metrohm 751 GPD Titrino using a combined Ag ring electrode, against a standardized $AgNO_3$ solution [63, 64].

Blank experiments were done in the dark in order to determine the contribution of electrolytic hydrogen production.

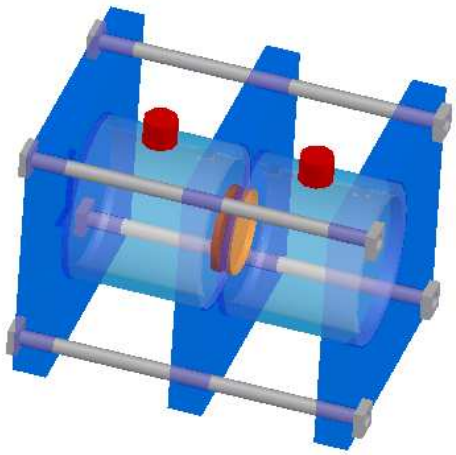

Fig. 2.1 Scheme of the photoelectrochemical cell.

2.3 Results and discussion

2.3.1 Scanning electron microscopy

SEM image of Bi_2AlNbO_7 film on 304 SS is shown in Fig. 2.1. The surface is fairly flat, with cracks distributed in all the area analyzed. The presence of cracks is due to the contraction of the film during the thermal treatment [65]. This feature was also observed in the other films.

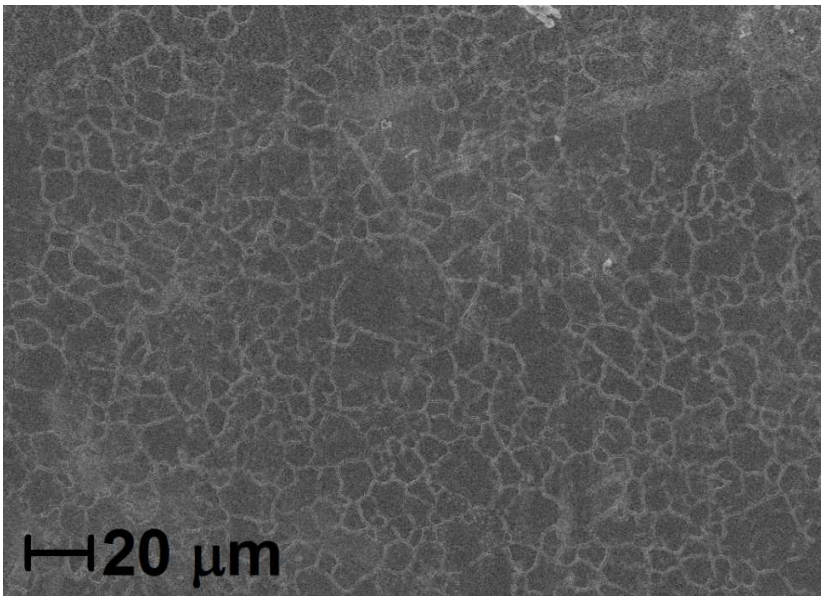

Fig. 2.2 SEM image of Bi_2AlNbO_7/304 SS (1000x).

2.3.2. X-ray diffraction

XRD patterns of Bi_2MNbO_7 (M = Al, Fe, Ga, In) films on 304 SS are shown in Fig. 3.3 Those of TiO_2 film on 304 SS and 304 SS annealed at 500℃ also were included for comparative purposes and as reference, respectively.

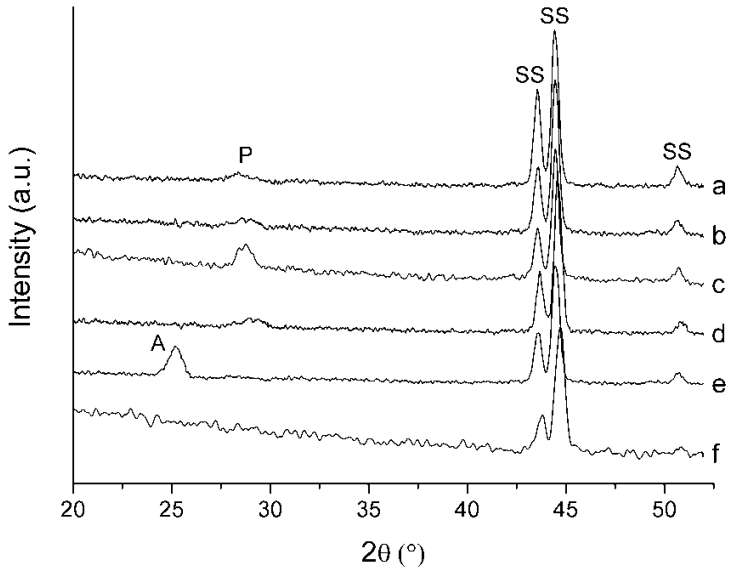

Fig. 2.3 XRD patterns of (a) Bi_2AlNbO_7/304 SS, (b) Bi_2FeNbO_7/304 SS, (c) Bi_2GaNbO_7/304 SS, (d) Bi_2InNbO_7/304 SS, (e) TiO_2/304 SS and (f) 304 SS.

In the XRD patterns of the Bi_2MNbO_7 films, only broad peaks at about 28.7° corresponding to the pyrochlore structure-type could be identified [57]. The intense reflections at 43.6, 44.6 and 50.7° correspond to the stainless steel support (Fig. 2.3f) [66]. It is strongly proposed that the broadening of the pyrochlore peaks is related to the small crystallite size and the low crystallinity [67]. Although all the Bi_2MNbO_7 films showed similar XRD patterns, the 2θ angles of the pyrochlore reflection: Bi_2AlNbO_7 (28.37°) < Bi_2FeNbO_7 (28.55°) < Bi_2GaNbO_7 (28.77°) < Bi_2InNbO_7 (28.91°) were slightly shifted according to the ionic radius of the 6-coordinated substituent atom M^{3+}: Al (67.5 pm) < Fe (69 pm) < Ga (76 pm) < In (94 pm) [68]. It is worth noting that the (101) anatase reflection at 25.21° in the XRD pattern of the TiO_2 film (Fig. 2.3e) is more defined that the corresponding pyrochlore reflections, indicating that the latter material achieves a higher crystallinity at the same annealing conditions. Previous reports indicated that the temperature to achieve the pyrochlore structure in the Bi-M-Nb-O system should be ≥900℃ when powders are prepared by solid state reaction [54, 55] while should be >400℃ when powders are prepared by the sol-gel method [58].

2.3.3. Energy dispersive X-ray fluorescence

EDXRF results of Bi_2MNbO_7 films on 304 SS are summarized in Table 2.1.

Table 2.1 Elemental analysis of the Bi_2MNbO_7/304 SS.

Film	Bi (at. %)	M (at. %)	Nb (at. %)
Bi_2AlNbO_7/304 SS	60.1	20.6	19.3
Bi_2FeNbO_7/304 SS	57.4	22.0	20.6
Bi_2GaNbO_7/304 SS	52.2	24.1	23.7
Bi_2InNbO_7/304 SS	63.3	18.8	17.9
Bi_2MNbO_7/304 SS [a]	50.0	25.0	25.0

[a] Stoichiometric ratio.

Elemental analyses indicate that the atomic percentages of Bi-Ga-Nb-O sample fit better to the stoichiometric ratio of pyrochlore-type structure (Bi_2MNbO_7). In the other samples a Bi excess was detected suggesting the presence of $Bi_5Nb_3O_{15}$ [58], $Bi_5In_2Nb_3O_{18-x}$ [69], Bi_2O_3/Bi_2O_{4-x} [70] or amorphous phases.

2.3.4. Photoelectrochemical evaluation of the materials

Preliminary experiments showed a significant increase in current density when Bi_2MNbO_7/304 SS immersed in alkaline solutions containing cyanide were illuminated. Current density values recorded over time during 1 h of the photoelectrochemical process by using Bi_2AlNbO_7/304 SS and Bi_2FeNbO_7/304 SS as photoanode, under UV-Vis illumination, in a solution 0.2 M KOH and 250 ppm CN^- (using 0.02 M KCl as supporting electrolyte) is shown in Fig. 2.4. The corresponding values by using TiO_2/304 SS and 304 SS as photoanode, under UV-Vis illumination, and Bi_2AlNbO_7/304 SS as anode, in the dark, were also included for comparative purposes.

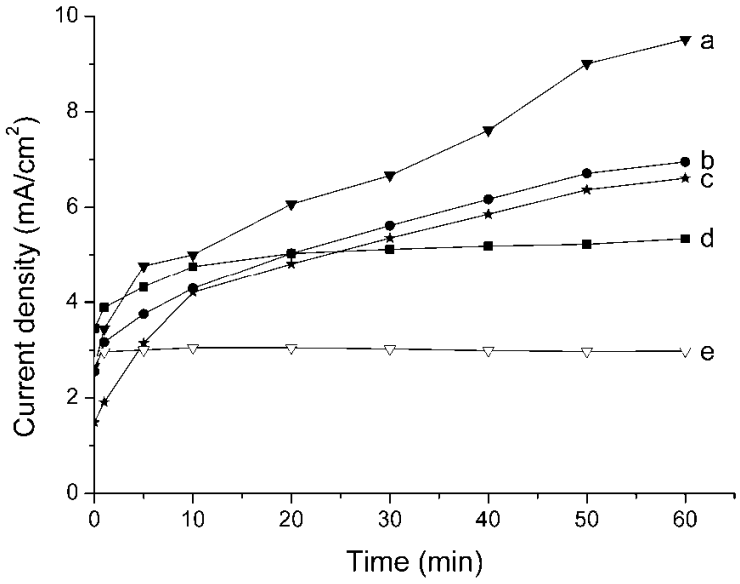

Fig. 2.4 Current density vs. time by using (a) Bi_2AlNbO_7/304 SS, (b) Bi_2FeNbO_7/304 SS, (c) TiO_2/304 SS and (d) 304 SS as photoanode, under UV-Vis illumination, and (e) Bi_2AlNbO_7/304 SS as anode, in the dark.

All Bi_2MNbO_7 films were more photoactive than TiO_2 film. Note that at the beginning of the process (t = 0) the current density obtained with 304 SS is higher than those obtained with the semiconductor films on 304 SS because the deposited material gives an electrical resistance to the electrical flux. This resistance is lower for Bi_2MNBO_7 films than TiO_2 film indicating that the former semiconductor family has a lower band-gap than TiO_2, as is shown in previous reports [56-59]. After 25 min, this barrier is overcome by the generation of photoelectrons and their subsequent transfer to the cathode (photogenerated current), resulting in increased current density and therefore an enhanced

hydrogen production [71, 72]. It is worth mentioning that 304 SS shows the same behavior with UV-Vis illumination and in the dark because it is a not photoactive material.

The values of accumulated current density and total amount of hydrogen produced after 1 h of the photoelectrochemical process by using Bi_2MNbO_7/304 SS, TiO_2/304 SS and 304 SS as photoanode, under UV-Vis illumination, in a solution 0.2 M KOH and 250 ppm CN^- (using 0.02 M KCl as supporting electrolyte) are summarized in Table 2.2. The values of accumulated current density were expressed quantitatively as the integral of the curves current density vs. time.

Table 2.2 Accumulated current density and total amount of hydrogen produced after 1 h of the photoelectrochemical process by using Bi_2MNbO_7/304 SS, TiO_2/304 SS and 304 SS as photoanode, under UV-Vis illumination.

Photoanode	Accumulated current density ($mA/cm^2 \times min$)	Total amount of hydrogen (μmol)
Bi_2AlNbO_7/304 SS	410.00	1.20
Bi_2FeNbO_7/304 SS	328.38	0.88
Bi_2GaNbO_7/304 SS	308.31	0.77
Bi_2InNbO_7/304 SS	330.25	0.89
TiO_2/304 SS	308.25	0.77
304 SS	299.05	0.68

It can be seen from the results in Table 2.2 that the accumulated current density has a direct relationship with the total amount of hydrogen produced, as expected in electrolytic processes. At the same electrolyte conditions and 1 h of the photoelectrochemical process the photoanodes exhibited the following performance: Bi_2AlNbO_7/304 SS >> Bi_2InNbO_7/304 SS ≈ Bi_2FeNbO_7/304 SS > Bi_2GaNbO_7/304 SS ≈ TiO_2/304 SS > 304 SS. These results can not be straightforward correlated with their band-gap values, degree of crystallinity or stoichiometric ratios as in the previous reports on photocatalytic degradation [59, 60]. Electrical and photoelectrical transport properties seem to play a preponderant role on these photoelectrochemical systems [54, 61]. Nevertheless, it is worth mentioning that nearly the same values of accumulated current density (about 180 $mA/cm^2 \times min$) and total amount of hydrogen produced (about

0.3 μmol) were obtained with all Bi_2MNbO_7 films during the electrochemical process in the dark.

On the other hand, each film exhibits the highest values of current density at different electrolyte conditions. These are presented in Table 2.3 together with the percentage of current increase by illumination, the hydrogen production rate and the cyanide conversion obtained after 3 h of the photoelectrochemical process. The percentage of current increase by illumination was calculated from the values of accumulated current density in the dark and under UV-Vis illumination. The hydrogen production rate was estimated from the linear regression slope of the graph total amount of hydrogen produced vs. time, shown in Fig. 2.5.

Table 2.3 Conditions employed and results obtained after 3 h of the photoelectrochemical process by using Bi_2MNbO_7/304 SS as photoanode, under UV-Vis illumination.

Photoanode	Electrolyte composition		Photoelectrochemical results		
	KOH (M)	CN^- (ppm)	Current increase by illumination (%)	H_2 production rate (μmol/min × 10^2)	CN^- conversion (%)
Bi_2AlNbO_7/304 SS	0.3	120	70.02	1.02	22.1
Bi_2FeNbO_7/304 SS	0.2	200	112.01	1.09	20.8
Bi_2GaNbO_7/304 SS	0.3	120	85.39	1.05	24.3
Bi_2InNbO_7/304 SS	0.3	200	142.94	1.31	25.2

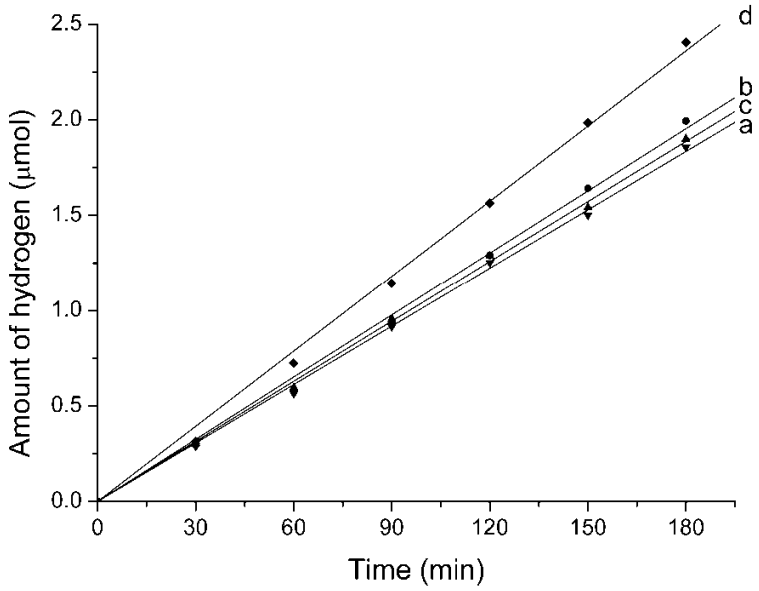

Fig. 2.5 Total amount of hydrogen produced vs. time by using (a) Bi_2AlNbO_7/304 SS, (b) Bi_2FeNbO_7/304 SS, (c) Bi_2GaNbO_7/304 SS and (d) Bi_2InNbO_7/304 SS as photoanode, under UV-Vis illumination.

It can be seen from the results in Table 2.3 that the percentage of current increase has a direct relationship with the hydrogen production rate, as is expected in photoelectrolytic processes. At different electrolyte conditions and 3 h of the photoelectrochemical process the photoanodes exhibited the following performance: Bi_2InNbO_7/304 SS >> Bi_2FeNbO_7/304 SS > Bi_2GaNbO_7/304 SS > Bi_2AlNbO_7/304 SS. Comparing Table 2.2 and 2.3, it can be clearly seen that further than optical or structural properties of the films, the semiconductor-electrolyte interface characteristics (determined by the electrolyte composition and concentration) govern their photoelectrochemical behavior. Finally, it is worth noting that the hydrogen production has a direct relationship with the cyanide oxidation, as is expected for the conjugated anodic reaction. This interdependence is not fulfilled with Bi_2FeNbO_7/304 SS because the oxidation of Fe^{2+} to Fe^{3+} could also take place in the film [73].

2.4. Conclusion

The activity of Bi_2MNbO_7/SS 304 photoanodes in the photoelectrochemical water splitting from alkaline solution containing cyanide was higher or equivalent than that of TiO_2/SS 304 photoanode.

Further than optical (band-gap values) or structural (degree of crystallinity, stoichiometric ratios) properties of Bi_2MNbO_7 films, the photoelectrical transport properties (intrinsic barrier to photoelectron transfer due to the interaction between the film and support) and the semiconductor-electrolyte interface characteristics (determined by the electrolyte composition and concentration) seem to have a major effect in their photoelectrochemical behavior.

The obtained results make further work on the photoelectrochemical application of Bi_2MNbO_7 films for both hydrogen production and water treatment very encouraging.

2.5. References

[1] Fujishima A, Honda K (1971) Bull Chem Soc Jpn 44:1148

[2] Fujishima A, Honda K (1972) Nature 37:238

[3] Fujishima A, Kohayakawa K, Honda K (1975) J Electrochem Soc 122:487

[4] Frank SN, Bard AJ (1977) J Am Chem Soc 99:303

[5] Frank SN, Bard AJ (1977) J Am Chem Soc 99:4667

[6] Frank SN, Bard AJ (1977) J Phys Chem 81:1484

[7] Nozik AJ (1978) Annu Rev Phys Chem 29:189

[8] Bard AJ (1979) J Photochem 10:59

[9] Grätzel M (1981) Acc Chem Res 14:376

[10] Pelizzetti E, Schiavello M (eds) (1991) Photochemical Conversion and Storage of Solar Energy. Kluwer, Dordrecht

[11] Bard AJ, Fox MA (1995) Acc Chem Res 28:141

[12] Schiavello M (ed) (1988) Photocatalysis and Environment: Trends and Applications. Kluwer, Dordrecht

[13] Ollis DF, Pelizzetti E, Serpone N (1991) Environ Sci Technol 25:1522

[14] Fox MA, Dulay MT (1993) Chem Rev 93:341

[15] Legrini O, Oliveros E, Braun AM (1993) Chem Rev 93:671

[16] Hoffmann MR, Martin ST, Choi W, Bahnemann DW (1995) Chem Rev 95:69

[17] Kamat PV (1993) Chem Rev 93:267

[18] Hagfeldt A, Grätzel M (1995) Chem Rev 95:49

[19] Thompson TL, Yates Jr. JT (2006) Chem Rev 106:4428

[20] Fujishima A, Zhang X, Tryk DA (2008) Surf Sci Rep 63:515
[21] Yates Jr. JT (2009) Surf Sci 603:1605
[22] Tryk DA, Fujishima A, Honda K (2000) Electrochim Acta 45:2363
[23] Nowotny J, Sorrell CC, Sheppard LR, Bak T (2005) Int J Hydrogen Energy 30:521
[24] Ni M, Leung MKH, Leung DYC, Sumathy K (2007) Renew Sust Energy Rev 11:401
[25] Matsuoka M, Kitano M, Takeuchi M, Tsujimaru K, Anpo M, Thomas JM (2007) Catal Today 122:51
[26] Fujishima A, Zhang X, Tryk DA (2007) Int J Hydrogen Energy 32:2664
[27] Linsebigler AL, Lu G, Yates Jr. JT (1995) Chem Rev 95:735
[28] Fujishima A, Rao TN, Tryk DA (2000) J Photochem Photobiol C Photochem Rev 1:1
[29] Carp O, Huisman CL, Reller A (2004) Prog Solid State Chem 32:33
[30] Rodríguez J, Candal RJ, Solís J, Estrada W, Blesa MA (2005) In: Blesa MA, Blanco Gálvez J (eds) Solar Safe Water: Tecnologías solares para la desinfección y descontaminación del agua, chapt 9. Escuela de Posgrado UNSAM, San Martín
[31] Hashimoto K, Irie H, Fujishima A (2005) Jpn J Appl Phys 44:8269
[32] Khan SUM, Al-Shahry M, Ingler Jr. WB (2002) Science 297:2243
[33] Niishiro R, Kato H, Kudo A (2005) Phys Chem Chem Phys 7:2241
[34] Kitano M, Tsujimaru K, Anpo M (2006) Appl Catal A General 314:179
[35] Sheppard LR, Bak T, Nowotny J, Nowotny MK (2007) Int J Hydrogen Energy 32:2660
[36] Singh AP, Kumari S, Shrivastav R, Dass S, Satsangi VR (2008) Int J Hydrogen Energy 33:5363
[37] Ye J, Zou Z, Arakawa H, Oshikiri M, Shimoda M, Matsushita A, Shishido T (2002) J Photochem Photobiol A Chem 148:79
[38] Kudo A (2003) Catal Surv Asia 7:31
[39] Wang J, Zou Z, Ye J (2005) J Phys Chem Solids 66:349

[40] Rajeshwar K (2008) In: Rajeshwar K, McConnell R, Licht S (eds) Solar Hydrogen Generation: Toward a Renewable Energy Future, chapt 7. Springer, New York

[41] Dhere NG, Bennur RS (2009) In: Gupta RB (ed) Hydrogen Fuel: Production, Transport, and Storage, chapt 7. CRC Press, Boca Raton

[42] Lee SG, Lee S, Lee HI (2001) Appl Catal A General 207:173

[43] Li Y, Lu G, Li S (2001) Appl Catal A General 214:179

[44] Lee K, Nam WS, Young Han G (2004) Int J Hydrogen Energy 29:1343

[45] Wu N-L, Lee M-S, Pon Z-J, Hsu J-Z (2004) J Photochem Photobiol A Chem 163:277

[46] Antoniadou M, Bouras P, Strataki N, Lianos P (2008) Int J Hydrogen Energy 33:5045

[47] Rader WS, Solujic L, Milosavljevic EB, Hendrix JL, Nelson JH (1995) Environ Pollut 90:331

[48] Augugliaro V, Loddo V, Marcì G, Palmisano L, López-Muñoz MJ (1997) J. Catal. 166:272

[49] Parga JR, Shukla SS, Carrillo-Pedroza FR (2003) Waste Manage 23:183

[50] Chiang K, Amal R, Tran T (2003) J Mol Catal A Chem 193:285

[51] Bozzi A, Guasaquillo I, Kiwi J (2004) Appl Catal B Environ 51:203

[52] Pedraza-Avella JA, Acevedo-Peña P, Pedraza-Rosas JE (2008) Catal Today 133-135:611

[53] Zou Z, Ye J, Abe R, Arakawa H (2000) Catal Lett 68:235

[54] Zou Z, Ye J, Arakawa H (2000) Solid State Commun 116:259

[55] Zou Z, Ye J, Arakawa H (2000) J Mater Sci Lett 19:1909

[56] Zou Z, Ye J, Arakawa H (2001) Chem Phys Lett 333:57

[57] Zou Z, Ye J, Arakawa H (2001) Mater Sci Eng B 79:83

[58] Garza-Tovar LL, Torres-Martínez LM, Bernal Rodríguez D, Gómez R, del Angel G (2006) J Mol Catal A Chem 247:283

[59] Ropero-Vega JL, Rosas-Barrera KL, Pedraza-Avella JA, Laverde-Cataño D, Pedraza-Rosas JE, Niño-Gómez ME (2010) Mater Sci Eng B 174:196

[60] Rosas-Barrera KL, Ropero-Vega JL, Pedraza-Avella JA, Niño-Gomez ME, Pedraza-Rosas JE, Laverde-Cataño DA (2010) Catal Today, accepted.

[61] Ropero-Vega JL, Sandoval-Páez JD, Pedraza-Avella JA, Vera-López E, Niño-Gómez ME, Ortiz-Otálora CA (2010) Thin Solid Films, submitted.

[62] Yoon KH, Noh JS, Kwon CH, Muhammed M (2006) Mater Chem Phys 95:79

[63] Eaton AD, Clesceri LS, Rice EW, Greenberg AE (2005) Standard Methods for the Examination of Water and Wastewater, 21st ed. American Public Health Association-American Water Works Association-Water Environment Federation, Baltimore. p 4-41

[64] Metrohm, Application Bulletin No. 46/2e

[65] Balasubramanian G, Dionysiou DD, Suidan MT, Subramanian V, Baudin I, Laîné JM (2003), J Mater Sci 38:823

[66] Sokolov S, Ortel E, Radnik J, Kraehnert R (2009) Thin Solid Films 518:27

[67] Arabatzis IM, Antonaraki S, Stergiopoulos T, Hiskia A, Papaconstantinou E, Bernard MC, Falaras P (2002) J Photochem Photobiol A Chem 149:237

[68] Huheey JE, Keiter EA, Keiter RL (1997) Química Inorgánica: Principios de estructura y reactividad, 4th ed. Oxford University Press, México. p 120

[69] Zou Z, Ye J (1999) J Alloys Compd 292:72

[70] Hameed A, Montini T, Gombac V, Fornasiero P (2008) J Am Chem Soc 130:9658

[71] Candal RJ, Rodríguez J, Colón G, Gelover S, Vigil Santos E, Jiménez A, Blesa MA (2004) In: Blesa MA, Sánchez B (eds) Eliminación de Contaminantes por Fotocatálisis Heterogénea, 2nd ed, chapt 7. CIEMAT, Madrid

[72] Bilmes SA, Candal RJ, Arancibia A, Loeb B, Rodríguez J (2004) In: Blesa MA, Sánchez B (eds) Eliminación de Contaminantes por Fotocatálisis Heterogénea, 2nd ed, chapt 8. CIEMAT, Madrid

[73] López T, Moreno JA, Gómez R, Bokhimi X, Wang JA, Yee-Madeira H, Pecchi G, Reyes P (2002) J Mater Chem 12:714

CHAPTER 3.

Photoelectrolytic hydrogen production using Bi_2MNbO_7 (M = Al, Ga) semiconductor film electrodes prepared by dip-coating

Abstract

The performance of Bi_2MNbO_7 (M = Al, Ga) films on AISI/SAE 304 stainless steel was evaluated in the photoelectrochemical hydrogen production as a function of the annealing temperature of the films (400, 500 and 600℃) and the composition of the electrolyte solution (containing KOH, KCN and KCl). The films were prepared by sol-gel dip-coating on AISI/SAE 304 stainless steel followed by a thermal annealing. The photoelectrochemical evaluation (UV-Vis, 2.5 V) was carried out in a conventional two-compartment electrochemical cell by using the prepared films as photoanode and a silver plate as cathode. During the process, circulating current was recorded and hydrogen production and cyanide degradation were measured. In both cases, it was found that the higher activity was obtained with the films annealed at 500℃ and using an electrolyte solution 0.3 M of KOH and 120 ppm of CN^-. Further works on the subject should involve a cathode evaluation to avoid the electrode polarization in presence of KCl and an experimental design to optimize the evaluated variables.

3.1 Introduction

Since Fujishima and Honda reported the photoelectrochemical water splitting using a TiO_2 electrode [1], many efforts has been made to synthesize visible-light responsive photocatalysts for the efficient use of solar energy [2]. On the other hand, other researchers have used electron donors as sacrificial agents (such as cyanide [3], oxalic acid [4], methanol [5] and iodide [6]), in order to achieve a higher efficiency, because they react with the photoinduced holes or the generated reactive oxygen species and in this way the electron-hole recombination is reduced.

Several investigations have been devoted on the modification of TiO_2 by doping [7-11] and current research is focused in the development of new semiconductor materials [12,13]. Among these Bi_2MNbO_7 (M = Al, Fe, Ga, Y, In, Rare Earth) are very promising photocatalysts [14-16]. They were prepared as powders initially by solid-state reaction [14-16] and then by the sol-gel method [17]. Our group has prepared Bi_2MNbO_7 (M = Al, Fe, Ga, In) films by sol-gel dip-coating on glass slides [18] and stainless steel [19] for the photocatalytic degradation of methyl orange and recently we have reported the preliminary evaluation of these latter on the photoelectrochemical hydrogen production from aqueous solution containing cyanide [20].

In this work, we evaluated the performance of the Bi_2MNbO_7 (M = Al, Ga) films on AISI/SAE 304 stainless steel in the photoelectrochemical water splitting for hydrogen production as a function of the annealing temperature of the films (400, 500 and 600℃) and the composition of the electrolyte solution (containing KOH, KCN and KCl).

3.2. Experimental

3.2.1. Materials

The following reagents were used as received without further purification: bismuth(III) acetate (Aldrich, 99.99%), aluminum(III) acetylacetonate (Aldrich, 99.999%), gallium(III) acetylacetonate (Aldrich, 99.99%), niobium(V) ethoxide (Aldrich, 99.95%), ethanol (Merck, 99.9%), acetylacetone (Aldrich, 99%), HNO_3 (Carlo Erba, 65%), 2-propanol (Merck, 99.5%), KOH (Carlo Erba, 85%), KCN (Aldrich, 97%), KCl (Merck, 99.5%), $AgNO_3$ (Carlo Erba, ACS-ISO for analysis), NaCl (Merck, 99.5%) and distilled water (> 1 MΩ·cm).

3.2.2. Preparation of the films

Semiconductor films of Bi-M-Nb-O (M = Al, Ga) system were prepared by the sol-gel dip-coating on AISI/SAE 304 stainless steel (SS) following the procedure described elsewhere [18]. In this process, stoichiometric quantities of the corresponding metal precursors (aluminum(III) or gallium(III) acetylacetonate) were mixed together with the complexing agent (acetylacetone), until a homogeneous alcoholic suspension was obtained. Later on, by hydrolysis and polycondensation reactions, a stable sol was formed and used for the preparation of the films on SS plates (1.5 cm × 2.5 cm). They were obtained at a withdrawal speed of 7.5 cm/min, dried at ambient temperature (25℃) for 20 min and finally annealed at 400, 500 or 600℃ for 4 h in air atmosphere.

3.2.3. Characterization of the films

X-ray diffraction (XRD) patterns were collected on a PANalytical X'Pert PRO diffractometer operated at 40 kV and 40 mA, using Cu Kα radiation (λ = 1.540598 Å) selected with Ni filter, in the thin film mode with a step of 0.02° and a counting time of 1.0 s per step.

Elemental analyses were performed by energy dispersive X-ray fluorescence (EDXRF) in a Shimadzu EDX-800HS spectrometer equipped with an Rh tube and a Si (Li) detector. The measurements were done in vacuum atmosphere and the quantification was performed using fundamental parameter method.

Scanning electron microscopy (SEM) was performed with a Leo 430 instrument operated at operated at 20 kV in secondary electron mode. The thickness of the films was measured by mounting the specimens in a perpendicular orientation on a thermo-hardening resin and which face was polished with alumina in order to obtain a plane surface.

UV-Vis transmission spectra of analogous films supported on glass slides were obtained using a Hewlett Packard 8453 spectrophotometer in the 800-200 nm range. They were used to estimate the band-gap energy (E_g) by extrapolation of the straight line from the absorption curve to the abscissa.

3.2.4. Photoelectrochemical evaluation of the films

The photoelectrochemical experiments were carried out in a 100 mL conventional cell with two cylindrical compartments (Diameter = 4 cm, Height = 4 cm). They were separated by an anion-permeable membrane (Ameridia Neosepta AMX), which avoids the mixture of gas products. As electrolyte solution, it was used an alkaline solution of KOH (0.1, 0.2, 0.3 or 0.4 M) containing CN^- (100, 120, 200 or 250 ppm) and KCl (0.01, 0.02 or 0.03 M). A traditional experimental method, varying one factor at a time and holding all other factors fixed, was used in this exploratory work. The Bi_2MNbO_7 (M = Al, Ga) films on SS were used as photoanode (Area = 3.75 cm^2) and a silver plate was used as cathode (Area = 3.75 cm^2). They were separated 2 cm and connected through a copper wire to a DC power supply (Hewlett Packard 6282A), which was used to apply a potential difference of 2.5 V during the experiments. Outer-irradiation was provided by a high pressure mercury-lamp (General Electric Kolorlux, 125 W), which emits UV-Vis radiation. A schematic representation of the system is shown in Fig. 3.1.

The potential difference was monitored and the circulating current was recorded every 10 min with a digital multimeter (Amprobe 30XR-A). The hydrogen

concentration in the headspace of the cathodic compartment (15 mL) was measured each 10 min during 1 h or each 30 min during 3 h with a gas analyzer (Crowcon Tetra, detection range: 0-100 ppm, detection limit: 1 ppm). The change in the cyanide concentration was determined by potentiometric titration (Metrohm 751 GPD Titrino, combined Ag ring electrode) against a standardized $AgNO_3$ solution [21,22].

Electrolysis experiments without illumination were carried out as a blank in order to determine the net contribution of the photocatalytic process.

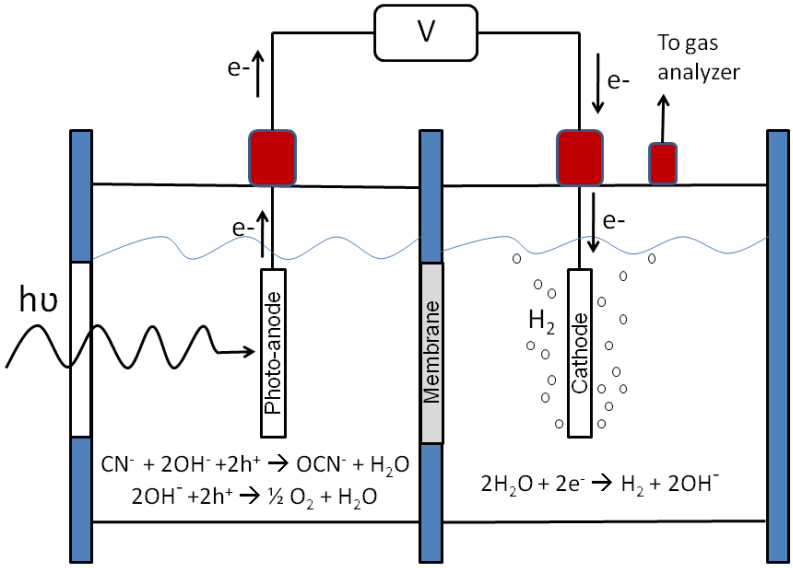

Fig. 3.1 Schematic representation of the photoelectrochemical system.

3.3. Results and discussion

3.3.1. Characterization of the films

XRD patterns of both materials showed a broad peak at about 28.7° when the annealing temperature was ≥ 500℃. These peaks appear at almost the same 2θ value than the given in the JCPDS card No. 053-1042 for the most intense reflection of Bi_2InNbO_7 suggesting a pyrochlore-type structure. The XRD patterns corresponding to the Bi_2AlNbO_7 films are shown in Fig. 3.2. The intense reflections at 43.6 and 44.6° are relate d to the SS support. It is worth noting that an increase in the annealing temperature from 500 to 600℃ allo ws obtaining films with higher

crystallinity, as it could be observed more clearly when the films were supported on indium tin oxide coated glass slides [23].

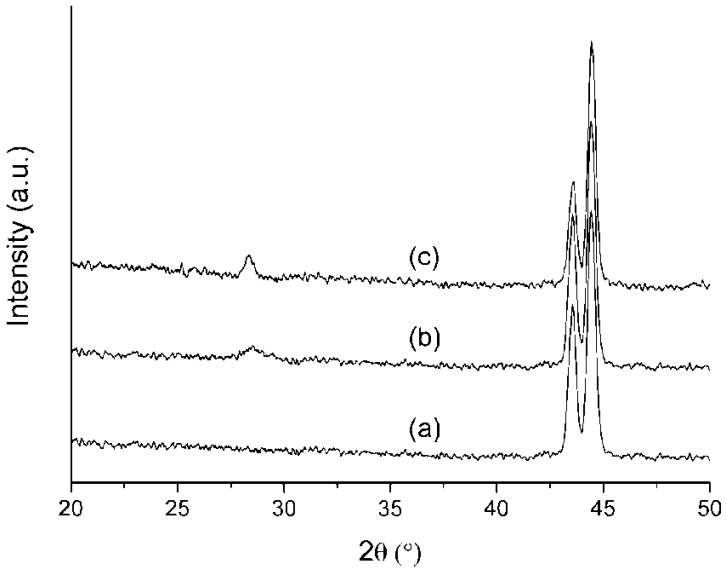

Fig. 3.2 XRD patterns of Bi_2AlNbO_7 films on SS annealed at (a) 400℃, (b) 500℃ and (c) 600℃.

EDXRF results of the prepared Bi_2MNbO_7 (M = Al, Ga) films on SS are summarized in Table 3.1.

Table 3.1. Elemental analyses of Bi_2AlNbO_7 and Bi_2GaNbO_7 films on SS annealed at different temperatures.

Annealing temperature (℃)	Bi_2AlNbO_7			Bi_2GaNbO_7		
	Bi (at. %)	Al (at. %)	Nb (at. %)	Bi (at. %)	Ga (at. %)	Nb (at. %)
400	62.4	19.7	17.9	54.8	22.7	22.5
500	60.1	20.6	19.3	52.2	24.1	23.7
600	58.9	21.3	19.8	51.5	24.6	23.9

It can be seen from Table 3.1 that when the annealing temperature was increased, the atomic percentages were fitted better to the stoichiometric ratio of Bi_2MNbO_7 in a pyrochlore-type structure (Bi: 50.0 at. %; Al, Ga and Nb: 25.0 at. %). These results appear in agreement with the previous findings obtained by XRD. Furthermore, the atomic percentages of the Bi-Ga-Nb-O films fitted better than those of the Bi-Al-Nb-O films. This behavior could be related to the stability of the sol prior to gelation. However, in both cases a Bi excess was detected, probably due to the dissimilar rates of dissociation of bismuth(III) acetate and complexation of bismuth(III) with acetylacetone in regard to the other precursors.

SEM micrographs of Bi_2AlNbO_7 films annealed at 500 and 600℃ are shown in Fig. 3.3

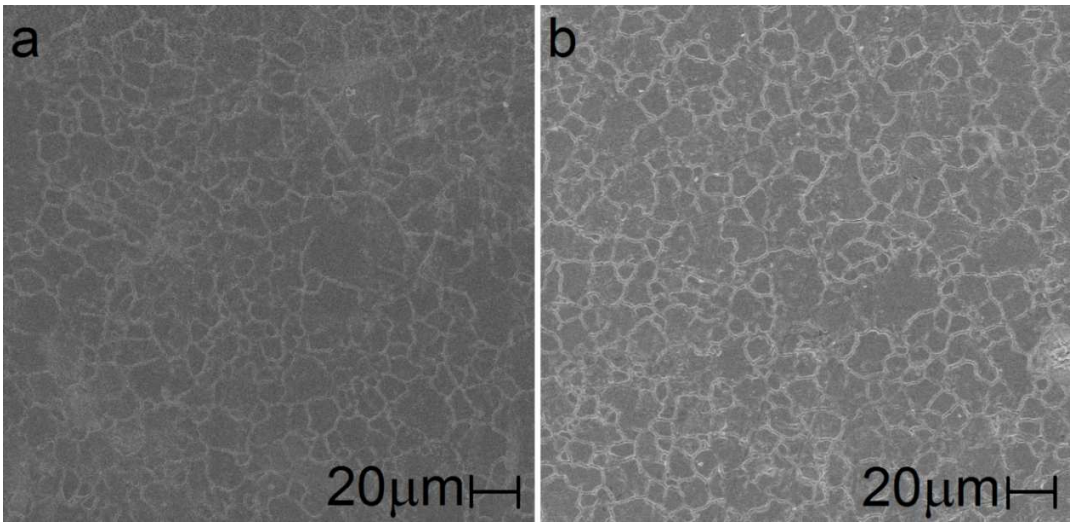

Figure 3.3. SEM micrographs (1000x) of Bi_2AlNbO_7 films on SS annealed at (a) 500℃ and (b) 600℃.

It can be seen from Fig. 3.3 that both films show a fairly but cracked surface. The film annealed at higher temperature (600℃) exhibit bigger cracks (see Fig. 3.3b) as a consequence of volume reduction (shrinkage) caused by grain coarsening with the increase of annealing temperature. The thickness of both films was about 4 μm.

The estimated E_g values were 2.79 eV for the Bi_2AlNbO_7 film and 2.67 eV for the Bi_2GaNbO_7 film, both annealed at 500℃. These films were able to absorb visible-light until 444 or 464 nm, respectively.

3.3.2. Photoelectrochemical evaluation of the films

Current density values versus time for the photoelectrochemical process carried out during 1 h by using Bi_2AlNbO_7/SS photoanodes annealed at 400, 500 and 600℃ in an electrolyte solution 0.2 M of KOH and 250 ppm of CN^- are shown in the Fig. 3.4. The corresponding values obtained in the dark by using Bi_2AlNbO_7/SS and SS anodes annealed at 500℃ were also included for comparative purposes.

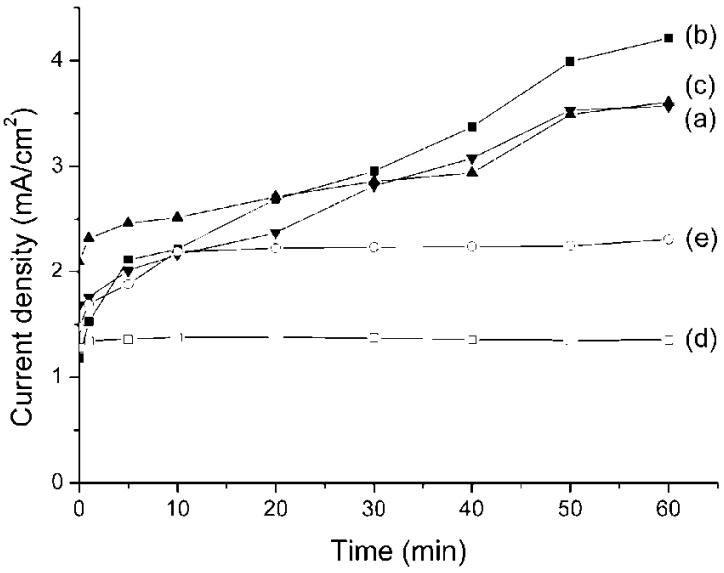

Fig. 3.4 Current density vs. time by using Bi_2AlNbO_7/SS photoanodes annealed at (a) 400℃, (b) 500℃ and (c) 600℃, under UV-Vis illumination, and (d) Bi_2AlNbO_7/SS and (e) SS anodes annealed at 500℃, in the dark. Electrolyte solution: 0.2 M KOH, 250 ppm CN^-.

It can be seen from Fig. 3.4 that under the same electrolyte conditions the higher current density was obtained with the film annealed at 500℃. The values of accumulated current density (which was expressed quantitatively as the integral of the curve current density vs. time) and total amount of hydrogen produced by using Bi_2AlNbO_7/SS electrodes are summarized in Table 3.2.

Table 3.2 Results of the photoelectrochemical process (1 h) by using Bi_2AlNbO_7/SS films annealed at different temperatures in an electrolyte solution 0.2 M KOH and 250 ppm of CN^-.

Anode	Accumulated current density ($mA/cm^2 \times min$)	Total amount of hydrogen (μmol)
Under UV-Vis illumination		
Bi_2AlNbO_7/SS (400℃)	166.29	0.272
Bi_2AlNbO_7/SS (500℃)	181.64	0.350
Bi_2AlNbO_7/SS (600℃)	174.82	0.298
In the dark		
Bi_2AlNbO_7/SS (500℃)	81.73	0.137
SS (500℃)	130.95	0.256

It can be seen from Table 3.2 that the accumulated current density has a direct relationship with the total amount of hydrogen produced, as expected in electrolytic processes. These results showed that the higher values of accumulated current density and total amount of hydrogen are obtained with the Bi_2AlNbO_7/SS photoanode annealed at 500℃. It is worth noting th at an increase in the annealing temperature from 400 to 500℃ implies a higher accu mulated current density and total amount of hydrogen, in accordance with the higher crystallinity (see Fig. 3.2). Although a further increment in the annealing temperature to 600℃ implies even a higher crystallinity, it has a detrimental effect probably because the specific surface area of the film was reduced. When the electrochemical process takes place in the dark, the values of accumulated current density and total amount of hydrogen significantly decrease, evidencing the importance of the photogenerated currents. Moreover, the values obtained with Bi_2AlNbO_7/SS (500℃) electrode in the dark are lower than those obtained with SS (500℃) electrode because the deposited material gives an electrical resistance to the electrical flux through the circuit.

In order to explore the conditions that lead to a higher hydrogen production, different electrolyte concentrations were evaluated and their results are shown in Table 3.3

Table 3.3. Results of the photoelectrochemical process (1 h) by using Bi_2AlNbO_7/SS and Bi_2GaNbO_7/SS films annealed at 500℃ in electrolyte solution s of different concentration.

Electrolyte concentration			Bi_2AlNbO_7/SS		Bi_2GaNbO_7/SS	
KOH (M)	CN^- (ppm)	KCl (M)	Accumulated current density ($mA/cm^2 \times min$)	Total amount of hydrogen (μmol)	Accumulated current density ($mA/cm^2 \times min$)	Total amount of hydrogen (μmol)
0.1	–	–	225.44	0.336	239.75	0.233
0.2	–	–	525.36	0.815	479.53	0.377
0.3	–	–	735.51	1.090	572.68	0.567
0.4	–	–	598.23	0.923	513.47	0.497
0.3	100	–	609.01	0.991	353.01	0.315
0.3	120	–	806.17	1.200	648.75	0.771
0.3	200	–	542.63	0.839	444.52	0.394
0.3	120	0.01	464.17	0.640	394.98	0.403
0.3	120	0.02	545.09	0.710	512.20	0.543
0.3	120	0.03	526.97	0.643	486.09	0.526

It can be seen from Table 3.3 that in the absence of CN^- and KCl, a KOH concentration of 0.3 M lead to the higher values in both accumulated current density and total amount of hydrogen produced. A further increment in the concentration of KOH to 0.4 M has a detrimental effect, probably because at higher pH the oxide surface is negatively charged and prevents the OH^- adsorption [24]. An addition of 100 ppm of CN^- also has a detrimental effect, probably because mass transfer limitations and the low adsorption of cyanide ions [25,26]. However, an addition of 120 ppm of CN^- has a positive effect, because the oxidation of CN^- is more feasible than OH^- oxidation [26]. A further increment in CN^- concentration to 200 ppm again has a detrimental effect, probably because desorption of OCN^- from the surface of photoanode is more difficult than desorption of O_2. In all cases, the

addition of KCl (0.01, 0.02 and 0.03 M) has a negative effect. Although this increases the conductivity of electrolyte solution, it reacts with the silver cathode forming AgCl at the surface, causing electrode polarization [27]. Among the evaluated electrolyte concentrations the most favorable was 0.3 M of KOH and 120 ppm of CN^-. The differences among Bi_2AlNbO_7/SS and Bi_2GaNbO_7/SS photoanodes can be attributed to their photoelectrical transport properties [23,28,29].

Keeping in mind that in the cathode occurs the hydrogen production (Eq. (1)) and in the photoanode occurs the oxidation of cyanide and hydroxide ions (Eqs. (2) and (3)), a photoelectrochemical process was carried out for 3 h by using Bi_2AlNbO_7/SS and Bi_2GaNbO_7/SS photoanodes annealed at 500℃ in an electrolyte solution 0.3 M of KOH and 120 ppm of CN^- in order to determine the hydrogen production rate (which was estimated from the linear regression slope of the graph: total amount of hydrogen produced vs. time, shown in Fig. 3.5) and the cyanide conversion. These results are shown in Table 3.4.

$$2H_2O + 2e^- \rightarrow H_2 + 2OH^- \quad (1)$$

$$2CN^- + 2OH^- + 2h^+ \rightarrow OCN^- + H_2O \quad (2)$$

$$OH^- + 2h^+ \rightarrow ½O_2 + H_2O \quad (3)$$

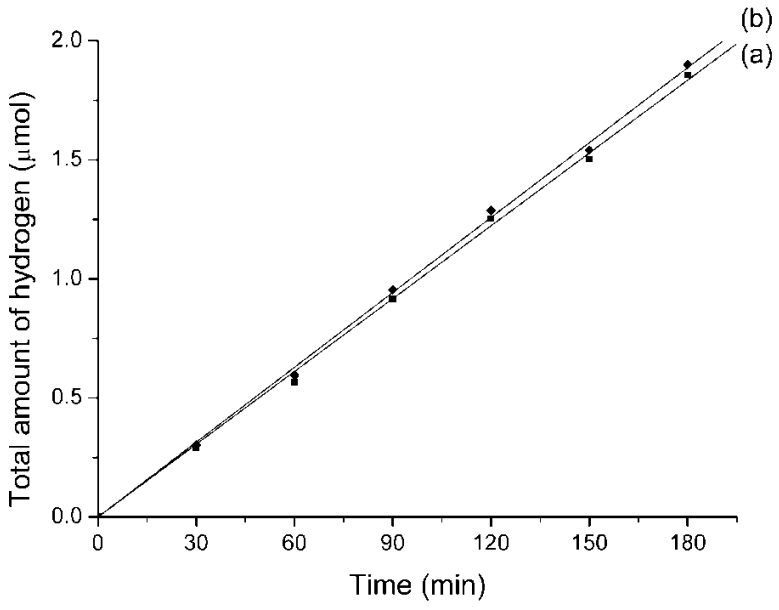

Fig. 3.5 Total amount of hydrogen produced vs. time by using (a) Bi_2AlNbO_7/SS and (b) Bi_2GaNbO_7/SS photoanodes annealed at 500℃, under UV-Vis ill umination. Electrolyte solution: 0.3 M KOH, 120 ppm of CN^-.

Table 3.4 Results of the photoelectrochemical process (3 h) by using Bi_2AlNbO_7/SS and Bi_2GaNbO_7/SS films annealed at 500℃ in an electrolyte solut ion 0.3 M KOH and 120 ppm of CN^-.

Anode	H_2 production rate ($\mu mol/min \times 10^2$)	CN^- conversion (%)
Bi_2AlNbO_7/SS	1.02	22.1
Bi_2GaNbO_7/SS	1.05	24.3

The results reported in Table 3.4 can be correlated with the proximity of the atomic percentages of the films to the stoichiometric ratio of Bi_2MNbO_7 in a pyrochlore-type structure as well as with the band-gap values of the films, such as in previous reports on photocatalytic degradation [18,19]. However, it is important to point out that the semiconductor-electrolyte interface characteristics (determined by the electrolyte composition and concentration) have a major effect in their photoelectrochemical behavior.

3.4 Conclusion

The activity of Bi_2MNbO_7/SS (M = Al, Ga) photoanodes in the photoelectrochemical hydrogen production from alkaline solution containing cyanide was higher than that of SS anode in an analogous electrochemical process in the dark.

It was found that the higher activity in the photoelectrochemical process was obtained with the photoanodes annealed at 500℃ and using an electrolyte solution 0.3 M of KOH and 120 ppm of CN^-.

Although Bi_2GaNbO_7/SS photoanode annealed at 500℃ exhibits a slightl y higher activity than the corresponding Bi_2AlNbO_7/SS photoanode after 3 h of the photoelectrochemical process, and this result are in agreement with the nearest atomic percentages to the stoichiometric ratio of Bi_2MNbO_7 in a pyrochlore-type structure and the lowest band-gap value, the photoelectrical transport properties (intrinsic barrier to photoelectron transfer due to the interaction between the film and support) and the semiconductor-electrolyte interface characteristics (determined by the electrolyte composition and concentration) seem to govern the photoelectrochemical behavior.

Further works on the subject should involve a cathode evaluation to avoid the electrode polarization in presence of KCl and an experimental design to optimize the evaluated variables.

3.5 References

[1] A. Fujishima, K. Honda, Nature 37 (1972) 238.

[2] J. Nowotny, C.C. Sorrell, L.R. Sheppard, T. Bak, Int. J. Hydrogen Energy 30 (2005) 521.

[3] S.G. Lee, S. Lee, H.I. Lee, Appl. Catal. A: General 207 (2001) 173.

[4] Y. Li, G. Lu, S. Li, Appl. Catal. A: General 214 (2001) 179.

[5] N.-L. Wu, M.-S. Lee, Z.-J. Pon, J.-Z. Hsu, J. Photochem. Photobiol. A: Chem. 163 (2004) 277.

[6] K. Lee, W.S. Nam, G. Young Han, Int. J. Hydrogen Energy 29 (2004) 1343.

[7] S.U.M. Khan, M. Al-Shahry, W.B. Ingler Jr., Science 297 (2002) 2243.

[8] R. Niishiro, H. Kato, A. Kudo, Phys. Chem. Chem. Phys. 7 (2005) 2241.

[9] L.R. Sheppard, T. Bak, J. Nowotny, M.K. Nowotny, Int. J. Hydrogen. Energy 32 (2007) 2660.

[10] M. Matsuoka, M. Kitano, M. Takeuchi, K. Tsujimaru, M. Anpo, J.M. Thomas, Catal. Today 122 (2007) 51.

[11] A.P. Singh, S. Kumari, R. Shrivastav, S. Dass, V.R. Satsangi, Int. J. Hydrogen Energy 33 (2008) 5363.

[12] K. Rajeshwar, in: K. Rajeshwar, R. McConnell, S. Licht (Eds.), Solar Hydrogen Generation: Toward a Renewable Energy Future, Springer, New York, 2008. pp. 167-228.

[13] N.G. Dhere, R.S. Bennur, in: R.B. Gupta (Ed.), Hydrogen Fuel: Production, Transport, and Storage, CRC Press, Boca Raton, 2009. pp. 227-282.

[14] Z. Zou, J. Ye, H. Arakawa, Mater. Sci. Eng. B 79 (2001) 83.

[15] Z. Zou, J. Ye, H. Arakawa, J. Phys. Chem. B 106 (2002) 517.

[16] Z. Zou, J. Ye, H. Arakawa, Int. J. Hydrogen Energy 28 (2003) 663.

[17] L.L. Garza-Tovar, L.M. Torres-Martínez, D. Bernal Rodríguez, R. Gómez, G. del Angel, J. Mol. Catal. A: Chem. 247 (2006) 283.

[18] J.L. Ropero-Vega, K.L. Rosas-Barrera, J.A. Pedraza-Avella, D.A. Laverde-Cataño, J.E. Pedraza-Rosas, M.E. Niño-Gómez, Mater. Sci. Eng. B 174 (2010) 196.

[19] K.L. Rosas-Barrera, J.L Ropero-Vega, J.A. Pedraza-Avella, M.E. Niño-Gomez, J.E. Pedraza-Rosas, D.A. Laverde-Cataño, Catal. Today (2011), doi:10.1016/j.cattod.2010.08.008.

[20] J.A. Pedraza-Avella, K.L. Rosas-Barrera, J.E. Pedraza-Rosas, D.A. Laverde-Cataño, Top. Catal. 54 (2011) 244.

[21] A.D. Eaton, L.S. Clesceri, E.W. Rice, A.E. Greenberg, Standard Methods for the Examination of Water and Wastewater, 21st ed. American Public Health Association-American Water Works Association-Water Environment Federation, Baltimore, 2005. p. 4-41.

[22] Metrohm, Application Bulletin No. 46/2e.

[23] J. Sandoval-Páez, J.L. Ropero-Vega, J. Bautista-Ruiz, C. Ortiz Otalora, E. Vera Lopez, J. Pedraza Avella, Rev. LatinAm. Metal. Mater. S1(3) (2009) 1057.

[24] A. Čop, D. Kovačević, T. Dragić, N. Kallay, Colloids Surf. A 230 (2003) 159.

[25] K. Chiang, R. Amal, T. Tran, J. Mol. Catal. A: Chem. 193 (2003) 285.

[26] J.A. Pedraza-Avella, P. Acevedo-Peña, J.E. Pedraza-Rosas Catal. Today 133 (2008) 611.

[27] G.T. Burstein, R.D.K. Misra, Electrochim. Acta 28 (1983) 363.

[28] Z. Zou, J. Ye, H. Arakawa, Solid State Commun. 116 (2000) 259.

[29] J.L. Ropero-Vega, J.D. Sandoval-Páez, J.A. Pedraza-Avella, E. Vera-López, M.E. Niño-Gómez, C.A. Ortiz-Otálora, in preparation.

CHAPTER 4.

Photoelectrocatalytic hydrogen generation and cyanide oxidation using Bi_2MNbO_7 (M = Fe, In) films on stainless steel

Abstract

The hydrogen production and the simultaneous cyanide oxidation by a photoelectrocatalytic process was studied using Bi_2MNbO_7 (M = Fe, In) films on AISI/SAE 304 stainless steel plates (SS) as photoanode. The films were prepared by sol-gel dip-coating and annealed at 500℃. A two-compartment electrochemical cell with a silver cathode was employed in the evaluation under different electrolyte compositions. The circulating current, the hydrogen generation and the cyanide degradation were monitored at different times. The higher activity was obtained by using 0.2 M of KOH and 200 ppm of CN^- for the Bi_2FeNbO_7/SS photoanode and 0.3 M of KOH and 200 ppm of CN^- for the Bi_2InNbO_7/SS photoanode. This result seems to be related with the surface charge at different pH values and the corresponding effect in the cyanide adsorption.

4.1 Introduction

Hydrogen can be produced by different process, inside those that the electrolysis of the water is feature due to that obtains hydrogen totally pure. The reaction that takes place during the process is,

$$H_2O \rightarrow {}^1/_2\, O_2 + H_2 \quad (1)$$

due to its endothermic nature this reaction requires input energy of 237 kJ/mol to it carried out [1]. However, Fujishima and Honda reported in 1972

the cleavage of water using TiO_2 semiconductor as photoanode in an electrochemical cell [2] without applying electric power. From then on, considerable interest has been devoted to photodecomposition of water as an alternative for solar energy conversion [3-5].

Photoelectrocatalytic processes using supported semiconductor materials as photoanodes is an advantage against using photocatalytic process. Since in a photoelectrochemical cell, an external potential is applied to the photoanode to promote the efficient separation of electron-hole pairs and accelerates the production of holes and $^{\bullet}OH$ as oxidizing species [6].

During the last decade, a series of semiconductor materials, Bi_2MNbO_7 (M= Al, Fe, Ga, In, Sm), were synthesized as powders, by a solid–state reaction [7] and a sol–gel process [8], and recently as films on glass slides, by sol–gel dip-coating [9]. This semiconductor has been evaluated in different reactions as photocatalytic hydrogen production and photodegradation of methylene blue.

Recently, our group prepared films of semiconductor oxides Bi_2MNbO_7 (M =Fe, In) which have shown visible light absorption and their photocatalytic activity in the degradation of methyl orange is higher or equivalent than the of TiO_2 films [10]. In this work, we explored the performance of the Bi_2MNbO_7 (M = Fe, In) films as a function of the electrolyte solution composition containing KOH, KCN and KCl

4.2 Experimental

4.2.1 Materials

The following reagents were used as received without further purification: bismuth(III) acetate (Aldrich, 99.99%), iron(III) acetylacetonate (Aldrich, 99.999%), indium(III) acetylacetonate (Aldrich, 99.99%), niobium(V) ethoxide (Aldrich, 99.95%), ethanol (Merck, 99.9%), acetylacetone (Aldrich, 99%), HNO_3 (Carlo Erba, 65%), 2-propanol (Merck, 99.5%), KOH (Carlo Erba, 85%), KCN (Aldrich, 97%),

KCl (Merck, 99.5%), $AgNO_3$ (Carlo Erba, ACS-ISO for analysis), NaCl (Merck, 99.5%) and distilled water (> 1 MΩ·cm).

4.2.2. Preparation of the films

Semiconductor films of Bi-M-Nb-O (M = Fe, In) system were prepared by sol-gel dip-coating on AISI/SAE 304 stainless steel (304 SS) plates. Briefly, an alcoholic suspension was made by mixing stoichiometric amounts of the corresponding metal precursors (iron(III) or indium(III) acetylacetonate), in the presence of a complexing agent (acetylacetone). Subsequently, by hydrolysis and polycondensation reactions, a stable sol was formed and used for the preparation of films on metallic substrates (15 mm × 25 mm), which were degreased by sonication in ethanol (15 min) and rinsed with distilled water. The films were made at a withdrawal speed of 7.5 cm/min. They were dried at room temperature (25℃) for 20 min and finally annealed at 500℃ for 4 h.

4.2.3. Characterization of the films

X-ray diffraction (XRD) patterns were collected on a PANalytical X'Pert PRO diffractometer operated at 40 kV and 40 mA, using Cu Kα radiation (λ = 1.540598 Å) selected with Ni filter, in the thin film mode with a step of 0.02° and a counting time of 2.0 s per step.

Elemental analyses were performed by energy dispersive X-ray fluorescence (EDXRF) in a Shimadzu EDX-800HS spectrometer equipped with an Rh tube and a Si (Li) detector. The measurements were done in vacuum atmosphere and the quantification was performed using fundamental parameter method.

UV-Vis transmission spectra of analogous films supported on glass slides were obtained using a Hewlett Packard 8453 spectrophotometer in the 800-200 nm range. They were used to estimate the band-gap energy (Eg) by extrapolation of the straight line from the absorption curve to the abscissa. Transparent glass slide was used as blank.

4.2.4. Photoelectrochemical evaluation of the films

The performance of the Bi_2MNbO_7 (M= Fe, In) films on 304 SS was evaluated by hydrogen production from aqueous solution. A 100 mL conventional cell with two cylindrical compartments (Diameter = 4 cm, Height = 4 cm) equipped with a high pressure mercury-lamp (General Electric Kolorlux, 125 W), which emits UV-Vis radiation, was employed in the photoelectrocatalytic experiments. The compartments were separated by an anion-permeable membrane (Ameridia Neosepta AMX), which avoids the mixture of gas products. In all tests,70 mL of alkaline solution of KOH (0.1, 0.2, or 0.3 M) containing CN^- (100, 200 or 300 ppm) and KCl (0.01, 0.02 or 0.03 M) were used as electrolyte. A traditional experimental method, varying one factor at a time and holding all other factors fixed, was used in this work.

The prepared films were used as photoanode and a silver plate (15 mm × 25 mm) was used as cathode. They were separated 2 cm and connected with a copper wire to a DC power supply (Hewlett Packard 6282A) operating at 2.5 V. The circulating current and potential differences applied on the electrodes were measured at least every 10 min during 1 to 3 h with an Amprobe 30XR-A digital multimeter. The hydrogen concentration in the headspace of the cathodic compartment (15 mL) was measured each 30 min during 1 to 3 h with a Crowcon Tetra gas analyzer (detection range: 0-1000 ppm, detection limit: 1 ppm). Finally, changes in the cyanide concentration in the anodic compartment (35 mL) were determined by potentiometric titration on a Metrohm 751 GPD Titrino using a combined Ag ring electrode, against a standardized $AgNO_3$ solution [11, 12].

Blank experiments were done in the dark in order to determine the contribution of electrolytic process.

4.3 Results and discussion

EDXRF results of the Bi_2MNbO_7 (M = Fe In) films on SS are summarized in Table 4.1.

Table 4.1. Elemental analysis of the Bi_2MNbO_7 (M = Fe, In) films on 304 SS.

Film	Bi (at. %)	M (at. %)	Nb (at. %)
Bi_2FeNbO_7	60.8	20.5	18.7
Bi_2InNbO_7	71.2	15.9	12.9
Bi_2MNbO_7*	50.0	25.0	25.0

* Stoichiometry ratio.

Elemental analyses indicate that the materials present a Bi excess, suggesting the formation of sometimes bismuth oxides as $Bi_5Nb_3O_{15}$ [8], $Bi_5In_2Nb_3O_{18-x}$ [7], Bi_2O_3/Bi_2O_{4-x} [13] or amorphous phases. it is possible to enhance the stoichiometric ratio of pyrochlore-type structure (Bi_2MNbO_7), fitting and controlling the speeds of the precursors' dissociation during the formation and stabilization of the sol in the sol-gel process. As well as, an appropriate modification in the thermal treatment of the films can influence significantly in the formation of the pyrochlore structure.

The estimated E_g values were 2.47 eV for the Bi_2FeNbO_7 film and 3.01 eV for the Bi_2InNbO_7 film, both annealed at 500℃. These films were abl e to absorb visible-light until 500 or 410 nm, respectively.

4.3.1. Photoelectrochemical evaluation of the materials

In order to explore the conditions that lead to a higher hydrogen production, different electrolyte concentrations were evaluated. Current density values versus time for photoelectrocatalytic process carried out during 1h by using Bi_2MNbO_7/SS (M = Fe, In) films in an electrolyte solution (0.1, 0.2 and 0.3 M of KOH) are shown in the Fig. 4.1 and 4.2.

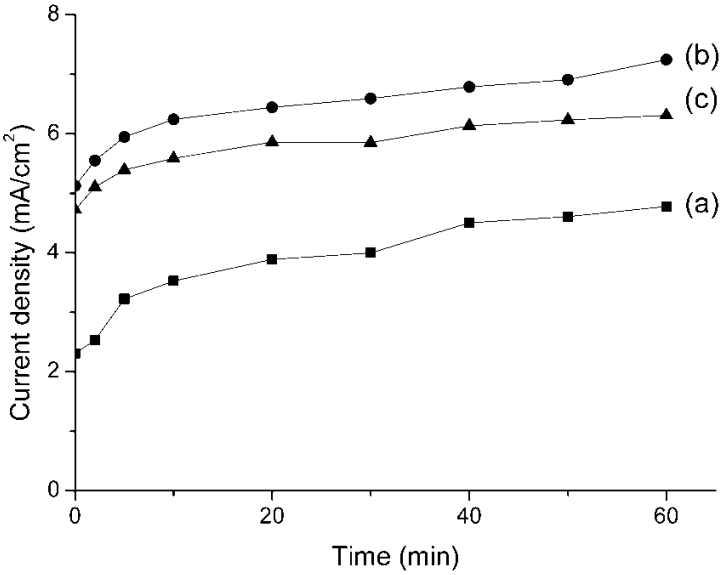

Fig. 4.1 Current density vs. time by using Bi_2FeNbO_7/SS as photoanode and (a) 0.1 M KOH, (b) 0.2 M KOH and (c) 0.3 M KOH as electrolyte solution.

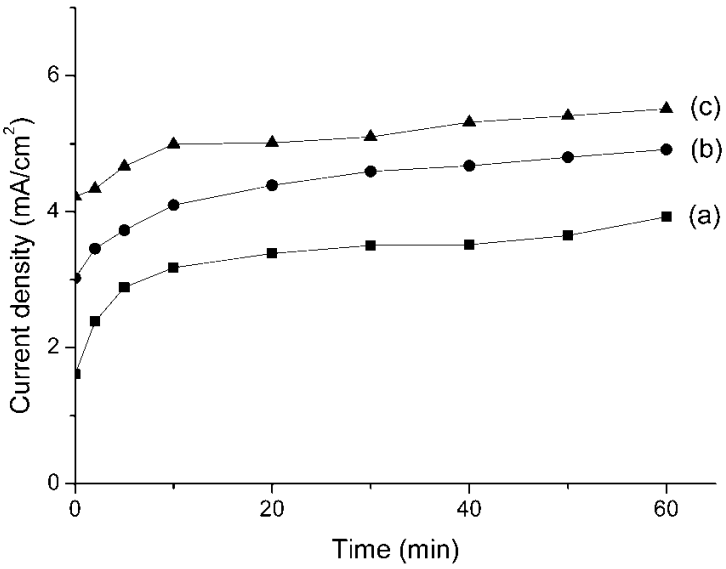

Fig. 4.2 Current density vs. time by using Bi_2InNbO_7/SS as photoanode and (a) 0.1 M KOH, (b) 0.2 M KOH and (c) 0.3 M KOH as electrolyte solution.

It can be seen from Fig. 4.1 and 4.2 than the current density values are higher when the KOH concentration is increased. Being a KOH concentration of

0.3 M the one that lead to the higher values in current density for Bi_2InNbO_7/SS. However, the Fig. 4.1 showed that a KOH concentration of 0.2 M exhibits slightly higher values in current density than 0.3 M of KOH for Bi_2FeNbO_7/SS. This increment of 0.2 to 0.3 M of KOH has a contrary effect probably because at higher pH the oxide surface is negatively charged and prevents the OH- adsorption [14].

In order to scavenge the coproduced O_2 and to hinder the reverse reactions, CN^- (100, 200 and 300 ppm) was added as oxidizing sacrifice agent to the alkaline electrolyte. Current density versus time after 1 h of photoelectrochemical process for Bi_2MNbO_7/SS (M = Fe, In) films is show in Fig. 4.3 and 4.4; as well as the higher results of current density obtained in last test.

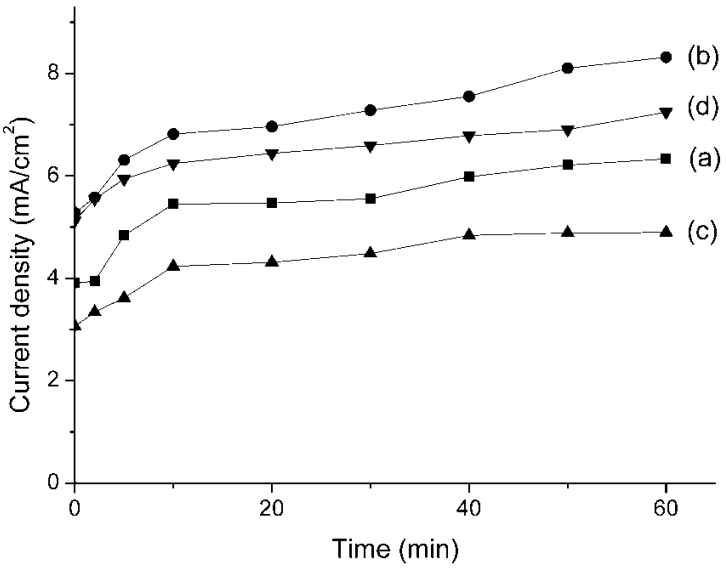

Fig. 4.3 Current density vs. time by using Bi_2FeNbO_7/SS as photoanode and (a) 0.2 M KOH + 100 ppm CN^-, (b) 0.2 M KOH + 200 ppm CN^-, (c) 0.2 M KOH + 300 ppm CN^- and (d) 0.2 M KOH as electrolyte solution.

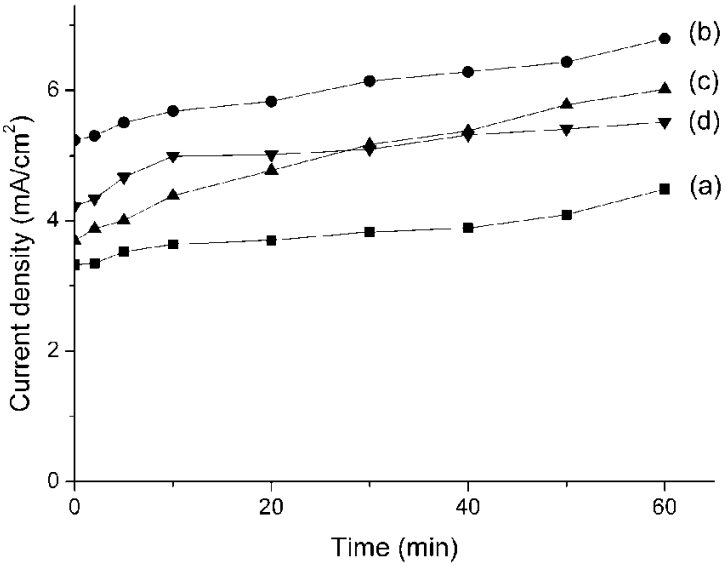

Fig. 4.4 Current density vs. time by using Bi_2InNbO_7/SS as photoanode and (a) 0.3 M KOH + 100 ppm CN^-, (b) 0.3 M KOH + 200 ppm CN^- and (c) 0.3 M KOH + 300 ppm CN^- and (d) 0.3 M KOH as electrolyte solution.

It can be seen from Fig. 4.3 and 4.4 that in both cases an addition of 100 ppm of CN^- has a detrimental effect, probably because mass transfer limitations and the low adsorption of cyanide ions [15, 16]. However, an addition of 200 ppm of CN^- has a positive effect, because the oxidation of CN^- is more feasible than OH^- oxidation [16]. A further increment in CN^- concentration to 200 ppm again has a detrimental effect, probably because desorption of OCN^- from the surface of photoanode is more difficult than desorption of O_2.

Finally, with purpose to decrease the losses due to ohmic electrolyte resistance KCl (0.01, 0.02 and 0.03 M) was added to the alkaline electrolyte. After of 1h of test, current density versus time is show in Fig. 4.5 and 4.6 for Bi_2MNbO_7/SS (M = Fe, In); as well as the higher results of current density obtained in last test.

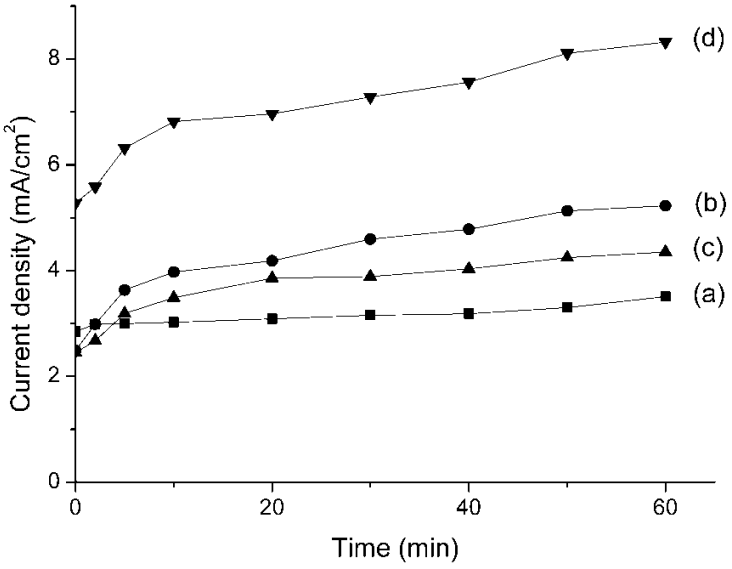

Fig. 4.5 Current density vs. time by using Bi_2FeNbO_7/SS as photoanode and (a) 0.2 M KOH + 200 ppm CN^- + 0.01 M KCl, (b) 0.2 M KOH + 200 ppm CN^-+ 0.02 M KCl and (c) 0.2 M KOH + 200 ppm CN^-+ 0.03 M KCl, and (d) 0.2 M KOH + 200 ppm CN^- as electrolyte solution.

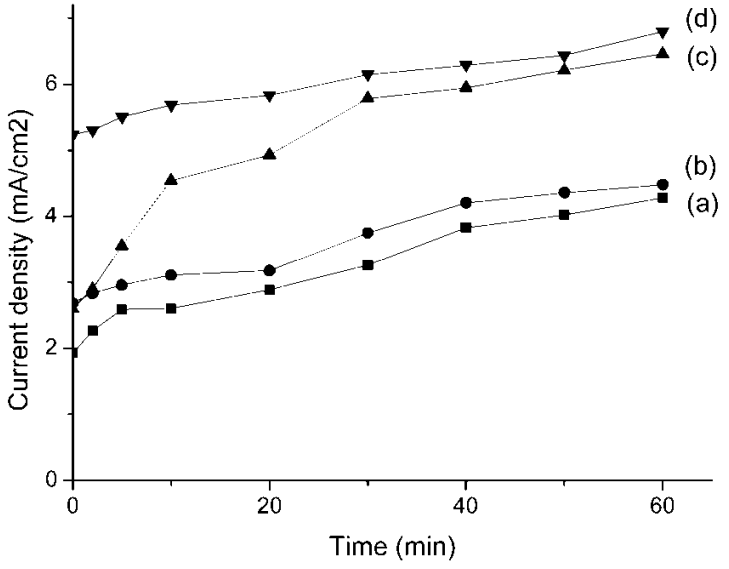

Fig. 4.6 Current density vs. time by using Bi_2InNbO_7/SS as photoanode and (a) 0.3 M KOH + 200 ppm CN^- + 0.01 M KCl, (b) 0.3 M KOH + 200 ppm CN^-+ 0.02 M KCl and (c) 0.3 M

KOH + 200 ppm CN^- + 0.03 M KCl and (d) 0.3 M KOH + 200 ppm CN^- as electrolyte solution.

As it is shown in the Fig. 4.5 and 4.6, the addition of 0.03 M of KCl allows a higher current density. However, in all cases the addition of KCl (0.01, 0.02 and 0.03 M) has a negative effect since it leads to a decreased in current density and hydrogen produced with regard to electrolyte without KCl. The other hand, although the addition of KCl increases the conductivity of electrolyte solution, it reacts with the silver cathode forming AgCl at the surface and causes electrode polarization [17].

The values of accumulated current density (which was expressed quantitatively as the integral of the curve current density vs. time) and the corresponding total amount of hydrogen produced by using Bi_2MNbO_7/SS (M = Fe, In) photoanodes the all test are summarized in Table 4.2

Table 4.2 Results of the photoelectrochemical process (1 h) by using Bi_2FeNbO_7/SS and Bi_2InNbO_7/SS films in electrolyte solutions of different concentration.

Electrolyte concentration			Bi_2FeNbO_7/SS		Bi_2InNbO_7/SS	
KOH (M)	CN^- (ppm)	KCl (M)	Accumulated current density ($mA/cm^2 \times min$)	Total amount of hydrogen (μmol)	Accumulated current density ($mA/cm^2 \times min$)	Total amount of hydrogen (μmol)
0.1	–	–	241.77	0.2052	203.08	0.3275
0.2	–	–	393.18	0.4531	266.42	0.3847
0.3	–	–	353.34	0.4275	307.21	0.4531
0.2-0.3	100	–	338.04	0.3933	230.78	0.5130
0.2-0.3	200	–	436.32	0.4702	364.14	0.8635
0.2-0.3	300	–	267.46	0.3505	303.52	0.5386
0.2-0.3	200	0.01	189.77	0.4275	198.89	0.4702
0.2-0.3	200	0.02	267.30	0.6241	222.21	0.5386
0.2-0.3	200	0.03	230.01	0.4788	319.20	0.5643

After testing the different electrolyte concentrations, the table 4.2 shows that the electrolyte solution 0.2 M of KOH and 200 ppm of CN^- for Bi_2FeNbO_7/SS and 0.3 M of KOH and 200 ppm of CN^- for Bi_2InNbO_7/SS presents the higher result of photoelectrocatalytic process in term of accumulated current density and total amount of hydrogen produced. The differences among photoanodes can be attributed to their photoelectrical transport properties [18, 19, 9].This table also suggests that the accumulated current density and total amount of hydrogen has a direct relationship as is expect in electrolytic process.

Keeping in mind that the photocatalytic process implies the use of the light energy to transform it into chemical energy, they were carried out tests during 3 h using Bi_2FeNbO_7/SS films annealed at 500℃, in the most favorable electrolyte concentration, in order to determine both current increase by illumination and hydrogen production rate. The percentage of current increase by illumination was calculated from the values of accumulated current density in the dark and under UV–Vis illumination. The hydrogen production rate was estimated from the linear regression slope of the graph total amount of hydrogen produced versus time, shown in Fig. 4.7 The results of current increase, hydrogen production rate and conversion of cyanide are summarized in table 4.3

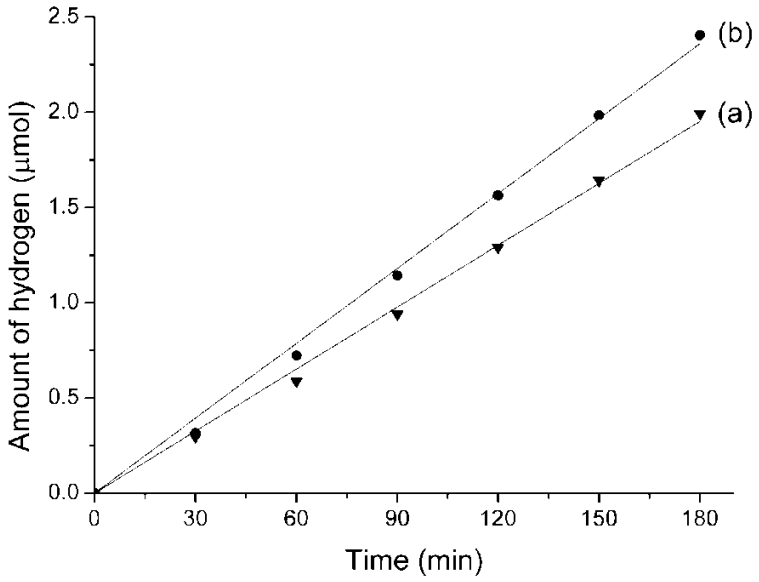

Fig. 4.7 Total amount of hydrogen produced vs. time by using (a) Bi_2FeNbO_7/SS in 0.2 M KOH + 200 ppm electrolyte and (b) Bi_2InNbO_7/SS in 0.3 M KOH + 200 ppm electrolyte as photoanode.

Table 4.3 Conditions and results using Bi_2MNbO_7 (M = Fe, In) films on 304 SS in the photoelectrochemical process at 2.5 V during 3 h.

Photoanode	Electrolyte concentration		Photoelectrochemical results		
	KOH [M]	CN^- [ppm]	Current increase [%]	H_2 production rate [μmol/min]	Cyanide oxidation [%]
Bi_2FeNbO_7	0.2	200	112.01	1.09	20.8
Bi_2InNbO_7	0.3	200	142.94	1.31	25.2

It can be seen from Table 4.3 that current increase of Bi_2InNbO_7 photoanode is approximately 27.6% higher than Bi_2FeNbO_7 photoanode. As well as, the higher hydrogen production rate and cyanide conversion. The results of hydrogen production and cyanide conversion are smaller than the expected in the

electrolytic process probably because the electrons generated in the Bi_2FeNbO_7 film is being used for oxidize herself of Fe^{+2} to Fe^{+3}.

4.4 Conclusions

It was found that the higher activity in the photoelectrochemical process was obtained using an electrolyte solution of 0.2 M of KOH and 200 ppm of CN^- for Bi_2FeNbO_7 photoanode and 0.3 M of KOH and 200 ppm for Bi_2InNbO_7 photoanode.

The activity of Bi_2InNbO_7/SS 304 photoanode in the photoelectrocatalytic hydrogen generation and cyanide oxidation was higher than that of Bi_2FeNbO_7/SS 304 photoanode.

It was found that the higher activity in the photoelectrocatalytic process is strongly influenced, if not determined, by the local properties of semiconductor-electrolyte interface and not by the photoelectrical transport characteristic.

Further works on the subject should involve the evaluation of another cathode material to avoid the electrode polarization in presence of KCl and an experimental design to optimize the evaluated variables.

4.5 References

[1] A. Kudo, Catal. Surv. Asia 7 (2003) 31-38
[2] A. Fujishima, K. Honda, Nature 37 (1972) 238.
[3] A.J. Bard, M.A. Fox. Acc. Chem. Res. 28 (1995) 141
[4] A.B. Murphy, P.R.F. Barnesa, L.K. Randeniya, I.C. Plumba, I.E. Greyb, M.D. Horneb, J.A. Glasscock, Int. J. Hydrogen Energy, 31 (2006) 1999.
[5] M. Ni, M.K.H. Leung, D.Y.C. Leung, K. Sumathy. Renew. Sust. Energy Rev. 11 (2007) 401.
[6] C.A. Martínez-Huitle, E. Brillas. Appl. Catal., B. Vol. 87. 2009. p.p. 105-145.

[7] Z. Zou, J. Ye, J. Alloys Compd 292 (1999) 72.
[8] L.L. Garza-Tovar, L.M. Torres-Martínez, D. Bernal Rodríguez, R. Gómez, G. del Angel, J. Mol. Catal. A: Chem. 247 (2006) 283.
[9] J.L. Ropero-Vega, K.L. Rosas-Barrera, J.A. Pedraza-Avella, D.A. Laverde-Cataño, J.E. Pedraza-Rosas, M.E. Niño-Gómez, Mater. Sci. Eng. B 174 (2010) 196.
[10] K.L. Rosas-Barrera, J.L. Ropero-Vega, J.A. Pedraza-Avella, M.E. Niño-Gómez, J.E. Pedraza-Rosas, D.A. Laverde-Cataño. Catal. Today. 166 (2011) 135.
[11] Eaton AD, Clesceri LS, Rice EW, Greenberg AE (2005) Standard Methods for the Examination of Water and Wastewater, 21st ed. American Public Health Association-American Water Works Association-Water Environment Federation, Baltimore. p 4-41
[12] Metrohm, Application Bulletin No. 46/2e
[13] A. Hameed, T. Montini, V. Gombac, P. Fornasiero, J. Am. Chem. Soc. 130 (2008) 9658.
[14] A. Čop, D. Kovačević, T. Dragić, N. Kallay, Colloids Surf. A 230 (2003) 159.
[15] K. Chiang, R. Amal, T. Tran, J. Mol. Catal. A: Chem. 193 (2003) 285.
[16] J.A. Pedraza-Avella, P. Acevedo-Peña, J.E. Pedraza-Rosas Catal. Today 133 (2008) 611.
[17] G.T. Burstein, R.D.K. Misra, Electrochim. Acta 28 (1983) 363.
[19] J. Sandoval-Páez, J.L. Ropero-Vega, J. Bautista-Ruiz, C. Ortiz Otalora, E. Vera Lopez, J. Pedraza Avella, Rev. LatinAm. Metal. Mater. S1(3) (2009) 1057.
[18] Z. Zou, J. Ye, H. Arakawa, Solid State Commun. 116 (2000) 259.

CHAPTER 5.

Hydrogen production by water splitting using Bi_2MNbO_7 (M = Al, Fe, Ga, In) films as photoanodes. A comparison between Ag, Pt and Pt/SS cathodes

Abstract

Cathodes of different materials (silver, platinum and platinized stainless steel) was evaluated in the hydrogen production by photoelectrochemical water splitting using Bi_2MNbO_7 (M = Al, Fe, Ga, In) films on stainless steel as photoanodes. Platinized stainless steel cathode was prepared by the Pechini method. Semiconductor Bi_2MNbO_7 (M = Al, Fe, Ga, In) films were prepared by sol-gel dip-coating on AISI/SAE 304 stainless steel plates and annealed at 500℃. The electrodes were immersed in an electrolyte solution containing KOH, KCN and KCl and during the process (UV-Vis, 2.5 V) circulating current, hydrogen production and cyanide degradation were measured. Platinum cathode allows avoiding the electrode polarization observed with silver cathode in the presence of KCl. however, in all cases the highest value of current density and amount of hydrogen produced was obtained using the platinized stainless steel. The Bi_2InNbO_7 film was the most active.

5.1. Introduction

It is well known that electrolysis of water is the preferred method to produce ultra pure hydrogen required in most of efficient fuel cells [1,2].Theoretically the electrolysis of pure water requires 1.23 V to produce hydrogen and oxygen.

However, in the practice an overpotential is needed to overcome various activation barriers. Without an excess energy the electrolysis of pure water occurs very slowly or not at all, limited by its poor electrical conductivity. Owing to various conductivity losses the applied voltage varies from 1.9 to as much as 3.0 V [3,4].

The efficiency in the electrolysis process can modify if one keeps in mind that the inherent inefficiency of the system depends on significantly of the electrodic materials and its capacity electrocatalytic to allow the reactions that happen on its surface:

$$2OH^- + 2h^+ \rightarrow {}^1/_2\, O_2 + H_2O\,(\text{anode}) \quad (1)$$

$$2H_2O + 2e^- \rightarrow H_2 + 2OH^-\,(\text{Cathode}) \quad (2)$$

The noble metals are the material most used in electrochemical, electrocatalysis, fuel cells and electroanalytic chemistry. Due to that these are inert to extremely positive potential and they have great ability to favor the adsorption of reagents and intermediary species formed during the reaction

Platinum is cathodic material most used in the hydrogen production. But due to high cost can be a good alternative to make platinum electrodes on a cheap substrate as long as they have the same electrochemical and chemical properties observed in the bulk material.

Some materials (as titanium) has been platinized and evaluated in organic compounds oxidation [5-7] and hydrogen production [8]. One of the methods used to manufacture the platinized electrodes is the polymeric precursor method (PPM) also called Pechini method [9,10]. Which is a simple and cheap route by obtain platinum electrodes. In Pechini method, a polymeric network, that containing the metallic ions, is obtained by metallic salts dissolving in a mixture of citric acid and ethylene glycol. After the substrate is painted with polymeric solution, the metallic films are obtained by an adequate thermal treatment.

In this chapter, platinized cathode was prepared on stainless steel 304 by Pechini method. The photoelectrochemical hydrogen production was evaluated and compared with Ag and Pt bulk in alkaline solution. The objective of this work is to decreased the platinum content of cathode material and avoid the polarization

Ag electrode when the support electrolyte as KCl is adding to alkaline solution. The Bi_2MNbO_7 (M = Al, Fe, Ga, In) films on SS were used as photoanode.

5.2. Experimental

5.2.1. Materials

The following reagents were used as received without further purification: bismuth(III) acetate (Aldrich, 99.99%), aluminum(III) acetylacetonate (Aldrich, 99.999%), gallium(III) acetylacetonate (Aldrich, 99.99%), indium(III) acetylacetonate (Aldrich, 99.99%), iron(III) acetylacetonate (Aldrich, 99.9%), niobium(V) ethoxide (Aldrich, 99.95%), ethanol (Merck, 99.9%), acetylacetone (Aldrich, 99%), HNO_3 (Carlo Erba, 65%), KOH (Carlo Erba, 85%), KCN (Aldrich, 97%), KCl (Merck, 99.5%), $AgNO_3$ (Carlo Erba, ACS-ISO for analysis), NaCl (Merck, 99.5%) and distilled water (1 MΩ·cm).

5.2.2. Preparation of the films

Semiconductor films of Bi-M-Nb-O (M = Al, Fe, Ga, In) system were prepared by sol-gel dip-coating on AISI/SAE 304 stainless steel (304 SS) plates. Briefly, an alcoholic suspension was made by mixing stoichiometric amounts of the corresponding metal precursors (the reagents mentioned above), in the presence of a complexing agent (acetylacetone). Details of the preparation have been described elsewhere [11]. Subsequently, by hydrolysis and polycondensation reactions, a stable sol was formed and used for the preparation of films on metallic substrates (15 mm × 25 mm), which were degreased by sonication in ethanol (15 min) and rinsed with distilled water. The films were made at a withdrawal speed of 7.5 cm/min. They were dried at room temperature (25℃) for 20 min and finally annealed in air at 500℃ for 4 h.

The Pt electrode was prepared using the polymeric precursor method on AISI/SAE 304 stainless steel substrates (15 mm × 25 mm). The precursor solution was prepared following the procedure described by Freitas *et al*.[1]. The precursor solution were painted onto the support (304 SS) with a brush and then it was

subjected to a thermal treatment at 130℃ for 30 mi n and then at 450℃ for 10 min to eliminate the organic compound and lead to the formation of metallic film.

5.2.3. Photoelectrochemical evaluation of the films

The photoelectrochemical experiments were carried out in a 100 mL conventional cell with two cylindrical compartments (Diameter = 4 cm, Height = 4 cm). They were separated by an anion-permeable membrane (Ameridia Neosepta AMX), which avoids the mixture of gas products. As electrolyte solution, it was used an alkaline solution (0.1-0.3 M KOH) containing cyanide as sacrificial reducing agent (100-300 ppm CN^-) and KCl (0.01-0.03 M) as electrolyte supporting. The Bi_2MNbO_7 (M = Al, Fe, Ga, In) films on SS were used as photoanode (Area = 3.75 cm^2), silver (Area = 3.75 cm^2), platinum (Area = 3.40 cm^2) and platinized stainless steel (Area = 3.75 cm^2) plates were used as cathodes. They were separated 2 cm and connected through a copper wire to a DC power supply (Hewlett Packard 6282A), which was used to apply a potential difference of 2.5 V during the experiments. Outer-irradiation was provided by a high pressure mercury-lamp (General Electric Kolorlux, 125 W), which emits UV-Vis radiation.

The potential difference was monitored and the circulating current was recorded every 10 min with a digital multimeter (Amprobe 30XR-A). The hydrogen concentration in the headspace of the cathodic compartment (15 mL) was measured each 10 min during 1 h or each 30 min during 3 h with a gas analyzer (Crowcon Tetra, detection range: 0-100 ppm, detection limit: 1 ppm). The change in the cyanide concentration was determined by potentiometric titration (Metrohm 751 GPD Titrino, combined Ag ring electrode) against a standardized $AgNO_3$ solution [12,13].

Electrolysis experiments without illumination were carried out as a blank in order to determine the net contribution of the photocatalytic process.

5.3. Results and discussion

5.3.1. Photoelectrochemical evaluation of the films

Percentage of current increase, hydrogen production rate and cyanide oxidation values, for the photoelectrochemical process carried out for 3 h by using Bi_2MNbO_7/SS (M = Al, Fe, Ga, In) photoanodes in alkaline solution using Pt as cathode are summarized in Table 5.1. The corresponding results obtained (in the previous chapters) using Ag cathode was also included for comparative purposes. The electrolyte concentration employed in this test was that where the highest values of accumulated current density and total amount of hydrogen produced (for each photoanode) were reached.

Table 5.1. Results of the photoelectrochemical process at 2.5 V during 3 h using Bi_2MNbO_7 (M = Al, Fe, Ga, In) films on 304 SS

Film	Ag cathode			Pt cathode		
	Current increase [%]	H_2 production rate [μmol/min × 10^2]	Cyanide oxidation [%]	Current increase [%]	H_2 production rate [μmol/min × 10^2]	Cyanide oxidation [%]
Bi_2AlNbO_7[1]	70.02	1.02	22.1	65.83	1.13	23.45
Bi_2FeNbO_7[2]	112.01	1.09	20.8	120.20	1.23	22.87
Bi_2GaNbO_7[A]	85.39	1.05	24.3	86.45	1.17	26.31
Bi_2InNbO_7[3]	142.94	1.31	25.2	130.12	1.64	29.43

It can be seen from the results in Table 5.1 that after 3 h of the photoelectrochemical process and used a platinum cathode, the photoanodes exhibited the following performance: Bi_2InNbO_7/304 SS >> Bi_2FeNbO_7/304 SS > Bi_2GaNbO_7/304 SS > Bi_2AlNbO_7/304 SS. as well as it has been showed in previous chapters. But the hydrogen production rate and cyanide oxidation has been higher that Ag cathode. It result is expected, since the Pt present a cathodic overpotential

[A] 0.3 M KOH + 120 ppm CN^- as electrolyte solution

[2] 0.2 M KOH + 200 ppm CN^- as electrolyte solution

[3] 0.3 M KOH + 200 ppm CN^- as electrolyte solution

smaller than Ag in the half reaction H^+/H_2 [14] and a great affinity with the water molecule.

On the other hand, with purpose to decrease the losses due to ohmic electrolyte resistance and taking advantage of that the platinum is very stable and extremely chemical inert metal, KCl (0.01, 0.02 and 0.03 M) was added to the alkaline electrolyte. After of 3h of photoelectrochemical process, current density versus time is showed in Fig. 5.1, using Bi_2FeNbO_7/SS as photoanode and Pt as cathode; as well as the highest value of current density obtained without KCl.

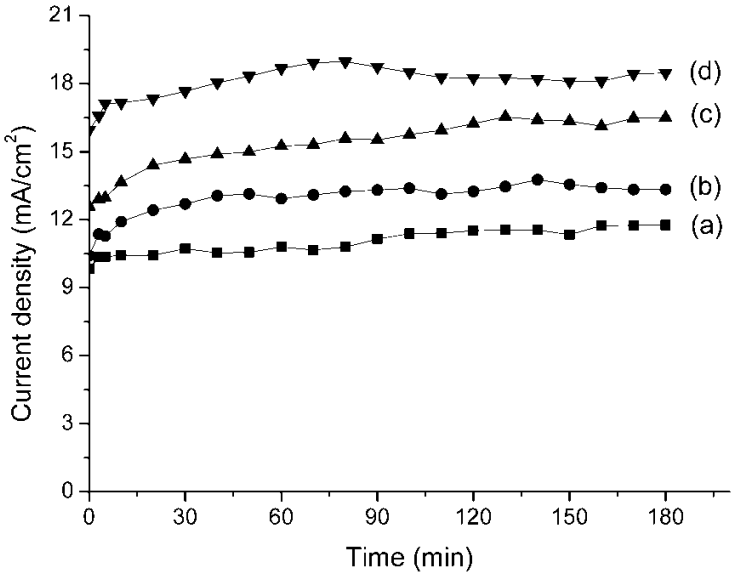

Fig. 5.1. Current density vs. time by using Bi_2FeNbO_7/SS as photoanode in electrolyte solution 0.2 M KOH + 200 ppm CN^- + (a) 0.00 M KCl, (b) 0.01 M KCl and (c) 0.02 M KCl, and (d) 0.03 M KCl.

As it is shown in the Fig. 5.1, in all cases the addition of KCl (0.01, 0.02 and 0.03 M) has a positive effect since it leads to an increased in current density and therefore hydrogen produced with regard to electrolyte without KCl. Furthermore, this result shows that, to difference of Ag electrode, the Pt electrode does not react with the potassium salt. It worth nothing mentioned that this behavior was obtained for the other materials.

As it is well know, the performance of the water splitting process is strongly influenced by the materials used as electrodes. The increases of accumulated current density and hydrogen production when the Pt cathode was changed by Pt/SS cathode during the photoelectrochemical process are show in the table 5.2.

Table 5.2. Increase of current density and total amount of hydrogen using Bi_2MNbO_7 (M = Al, Fe, Ga, In) films on 304 SS as photoanode. Comparison between Pt and Pt/SS

Film	Photoelectrochemical results	
	Increase of current density [%]	Increase of total amount of hydrogen [%]
Bi_2AlNbO_7[4]	27.5	11.2
Bi_2FeNbO_7[5]	33.6	16.3
Bi_2GaNbO_7[D]	29.3	13.4
Bi_2InNbO_7[6]	38.1	18.1

As it can be seen from table 5.2, in all cases the used of platinized stainless steel has a positive effect over photoelectrolytic process. Since it causes an increment of until 38.1 percent in the current density and an increment of until 18.1 percent in the total amount of hydrogen produced. This positive effect causes by Pt/SS is not yet clear but can be attributed to the change in the energy surface due to a change of the crystallographic orientation and lattice stresses observed in the substrate [15].

5.4. Conclusions

After 3 h of the photoelectrochemical process, the use of a platinum cathode in an alkaline solution (without KCl) shows higher values of hydrogen production rate and cyanide oxidation with regard to obtained results with Ag cathode.

[D] 0.3 M KOH + 120 ppm CN^- + 0.03 M KCl as electrolyte solution

[5] 0.2 M KOH + 200 ppm CN^- + 0.03 M KCl as electrolyte solution

[6] 0.3 M KOH + 200 ppm CN^- + 0.03 M KCl as electrolyte solution

The addition of 0.03 M of KCl as support electrolyte leads to an increase of the accumulated current density and hydrogen production. This result we suggest that the platinum cathode allows avoiding the electrode polarization observed with silver cathode in the presence of KCl.

Finally, in all cases the highest value of current density and amount of hydrogen produced was obtained using the platinized stainless steel as cathode. Being the Bi_2InNbO_7 photoanode the most active.

5.5. References

[1] B. C. H. Steele, A. Heinzel. Nature 414 (2001) 345.

[2] A. Kundu, J.H. Jang.Encyclopedia of Electrochemical Power Sources (2009) 39-45.

[3] J.O.M. Bockris, K. Uosaki, H. Kita. J Appl Phys 52 (1981) 808.

[4] A.J. Bard, M.A. Fox. Acc. Chem. Res. 28 (1995) 141

[5] R.G. Freitas, R.T.S. Oliveira, M.C. Santos, L.O.S. Bulhões, E.C. Pereira. Mater. Lett. 60 (2006) 1906.

[6] R.G. Freitas, M.C. Santos, R.T.S. Oliveira, L.O.S. Bulhões, E.C. Pereira. J. Power Sources 158 (2006) 164.

[7] R.G. Freitas a, L.F. Marchesi a, R.T.S. Oliveira, F.I. Mattos-Costa, E.C. Pereira, L.O.S. Bulhões, M.C. Santos. J. Power Sources 171 (2007) 373.

[8] C. Sang-Youn, B.Y. Jyotiprakash, K. Kang-Jin, J. Oh-Shim. Int. J. Hydrogen Energy 36 (2011) 3347.

[9] M. Kakihana, J. Sol-Gel Sci. Technol. 6 (1996) 7.

[10] P.M. Pechini, United States Patent Office, 3 330 697, 1967.

[11] J.L. Ropero-Vega, K.L. Rosas-Barrera, J.A. Pedraza-Avella, D.A. Laverde-Cataño, J.E. Pedraza-Rosas, M.E. Niño-Gómez, Mater. Sci. Eng. B 174 (2010) 196.

[12] Eaton AD, Clesceri LS, Rice EW, Greenberg AE (2005) Standard Methods for the Examination of Water and Wastewater, 21st ed. American Public Health Association-American Water Works Association-Water Environment Federation, Baltimore. p 4-4.
[13] Metrohm, Application Bulletin No. 46/2e
[14] J. Tafel, "Zeitschrift fur physikalische Chemie", 50 (1905) 641.
[15].W.D. Kingery, H.K. Bowen, D.R. Uhlmann, Introduction to Ceramics, 2nd ed., John Wiley and Sons, 1976, p. 448 (Chapter 10).

General Conclusions

In this thesis, the performance of a series of semiconductor materials for hydrogen production by photoelectrochemical process was made, highlighting the following conclusions:

The photodegradation of MeO increase with a faster withdrawal speed and with increases of the number of layer deposited. Degradation of MeO follows an apparent first order kinetics as most of the pollutant, which confirm the heterogeneous catalytic character of system for diluted solution. Furthermore, the photoactivity of Bi_2MNbO_7 films was higher or equivalent than TiO_2 films and the Bi_2GaNbO_7 film has the major cristallinity and the best elemental proportion according to pyrochlore-type structure.

The activity of Bi_2MNbO_7/SS (M = Al, Ga) in the photoelectrochemical hydrogen production from alkaline solution containing cyanide was obtained with the photoanodes annealed at 500℃ and depend of the electrolyte composition and concentration.

The activity of Bi_2MNbO_7/SS (M = Al, Fe, Ga, In) photoanodes in the photoelectrochemical water splitting from alkaline solution containing cyanide was higher or equivalent than that of TiO_2/SS 304 photoanode.

Further than optical (band-gap values) or structural (degree of crystallinity, stoichiometric ratios) properties of Bi_2MNbO_7 films, the photoelectrical transport properties (intrinsic barrier to photoelectron transfer due to the interaction between the film and support) and the semiconductor-electrolyte interface characteristics (determined by the electrolyte composition and concentration) seem to have a major effect in their photoelectrochemical behavior.

The addition of 0.03 M of KCl as support electrolyte leads to an increase of the accumulated current density and hydrogen production. This result we suggest that the platinum cathode allows avoiding the electrode polarization observed with silver cathode in the presence of KCl.

Finally, in all cases the highest value of current density and amount of hydrogen produced was obtained using the platinized stainless steel. Being the Bi_2InNbO_7 film was the most active.

LIST OF PUBLICATIONS

In press

Photoelectrolytic hydrogen production using Bi2MNbO7 (M = Al, Ga) semiconductor film electrodes prepared by dip-coating

In press: K.L. Rosas-Barrera, et al., Mater. Sci. Eng. B (2011), doi:10.1016/j.mseb.2011.05.048

Published

Photoelectrochemical hydrogen production from aqueous solution containing cyanide using Bi_2MNbO_7 (M = Al, Fe, Ga, In) films on stainless steel as photoanodes

Topics in Catalysis 54 (2011) 244–249

Photocatalytic degradation of methyl orange using Bi_2MNbO_7 (M= Al, Fe, Ga, In) semiconductor films on stainless steel

Catalysis Today 166 (2011) 135–139

Photophysical and photocatalytic properties of Bi_2MNbO_7

(M = Al, In, Ga, Fe) transparent thin films prepared by dip-coating

Materials Science and Engineering B 174 (2010) 196–199

Symposia and congress

Photoelectrochemical hydrogen production using Bi2MNbO7 (M= In, Fe) films as photo-anodes.

Fifth San Luis Symposium on Surfaces, Interfaces and Catalysis, *poster Presentation*

April 9 -19, 2010, sao Pedro, Brazil.

Photocatalytic degradation of methyl orange Using a new family of semiconductor Bi_2MNbO_7 (M = Al, In, Ga, Fe) thin films

XVIII International Materials Research congress, *Oral Presentation*

August 16-21, 2009, Cancun, Quintana Roo, Mexico.

Metal oxide photoelectrodes of Bi_2MNbO_7 (M = Al, Ga) for hydrogen production by water splitting

XIX Internacional Materials Research congress, *Poster Presentation*

August 15-19, 2010, Cancun, Quintana Roo, Mexico.

Hydrogen generation by water splitting using semiconductor Bi_2MNbO_7 (M= Al, In, Ga, Fe) films as photoanodes

XIV Internacional Materials Research congress, *Poster Presentation*

August 15-19, 2010, Cancun, Quintana Roo, Mexico.

Evaluación de películas semiconductoras de Bi_2MNbO_7 (M= Al, Ga) en la producción de hidrógeno mediante electrólisis fotoasistida de agua

V Congreso internacional de materiales, *Presentación Oral*

Octubre 12-16, 2009, Cali, Colombia.

Producción de hidrógeno mediante foto-electrólisis de agua, usando películas de tipo pirocloro Bi_2MNbO_7 (M= In, Fe) soportadas sobre acero inoxidable AISI-SAE 304.

V Congreso internacional de materiales, *Presentación Poster*

Octubre 12-16, 2009, Cali, Colombia.